Review: Geothermal heat as a tracer of large-scale groundwater flow and as a means to determine permeability fields

Martin O. Saar

Abstract A review of coupled groundwater and heat transfer theory is followed by an introduction to geothermal measurement techniques. Thereafter, temperature-depth profiles (geotherms) and heat discharge at springs to infer hydraulic parameters and processes are discussed. Several studies included in this review state that minimum permeabilities of approximately $5\times10^{-17}<k_{min}<10^{-15}m^2$ are required to observe advective heat transfer and resultant geotherm perturbations. Permeabilities below k_{min} tend to cause heat-conduction-dominated systems, precluding inversion of temperature fields for groundwater flow patterns and constraint of permeabilities other than being $<k_{min}$. Values of k_{min} depend on the flow-domain aspect-ratio, faults and other heterogeneities, anisotropy of hydraulic and thermal parameters, heat-flow rates, and the water-table shape. However, the k_{min} range is narrow and located toward the lower third of geologic materials, which exhibit permeabilities of $10^{-21}<k<10^{-7}m^2$. Therefore, a wide range of permeabilities can be investigated by analyzing subsurface temperatures or heat discharge at springs. Furthermore, temperature is easy and economical to measure and because thermal material properties vary far less than hydraulic properties, temperature measurements tend to provide better-constrained groundwater flow and permeability estimates. Aside from hydrogeologic insights, constraint of advective/conductive heat transfer can also provide information on magmatic intrusions, metamorphism, ore deposits, climate variability, and geothermal energy.

Keywords Review · Geothermal · Heat · Tracer · USA

Received: 15 March 2010 / Accepted: 18 September 2010
Published online: 25 November 2010

M. O. Saar (✉)
Department of Geology and Geophysics,
University of Minnesota,
310 Pillsbury Dr. SE, Minneapolis, MN 55455, USA
e-mail: saar@umn.edu
Tel.: +1-612-6257332
Fax: +1-612-6256541

Introduction and scope

For the last 50 years, it has been recognized that geothermal heat can serve as a natural tracer of groundwater flow (e.g., Suzuki 1960; Stallman 1963; Bredehoeft and Papadopulos 1965; Stallman 1965). More recently, Mary P. Anderson published a review paper on the topic (Anderson 2005), which serves as a general basis for the more specific discussion presented here. The goal of this contribution is to focus discussion on coupled groundwater and heat transfer at the watershed to regional scale. Its scope extends from interpretation of deep temperature-depth (geotherm) profiles to near-surface groundwater and heat transfer features that are indicative of large-scale groundwater flow patterns and rates.

This focus on large-scale groundwater flow systems is motivated by increasing recognition that groundwater flow models at these scales need to be constrained by multiple diverse observations beyond hydrologic data—including heat but potentially also solutes such as noble gases or isotopes (e.g., Woodbury et al. 1987; Woodbury and Smith 1988; Bravo et al. 2002). Indeed, Anderson (2005) states that "It is generally recognized that [hydraulic] head data alone are not sufficient to calibrate a ground water flow model, while estimates of ground water flux and/or information on the movement of solute and/or heat help constrain the calibration." As the topic of this paper is use of heat as a natural tracer, solutes will not be discussed in detail.

Multiphase systems or hydrothermal systems within oceanic crust (e.g., at mid-ocean ridges) are also only peripheral here, as the focus is on heat as a tracer of groundwater flow in continental-crust systems in general, rather than on high-temperature multiphase magmatic hydrothermal systems in particular. Nonetheless, many examples discussed in the following refer to volcanically and/or tectonically active regions, as single-phase fluid flow may often be assumed in moderate-temperature geothermal regions (e.g., Ingebritsen et al. 1992). For a recent review on the modeling of multiphase, multicomponent magmatic hydrothermal systems, including oceanic-crust systems, the reader is referred to Ingebritsen et al. (2010).

Finally, as this contribution focuses on characterizing watershed to regional flow systems, surface–groundwater interactions, including permafrost thawing, are little

 DOI 10.1007/s10040-010-0657-2

discussed. More emphasis is given to the use of spring data to constrain large-scale flow patterns. The review paper by Anderson (2005) is mainly devoted to coupled water and heat-flow processes that act near the land surface. Stonestrom and Constantz (2003) and Constantz (2008) also review using heat as a tracer to determine streambed water exchanges, while the effects of thawing permafrost are discussed in several other, recent publications (e.g., McKenzie et al. 2007; Walvoord and Striegl 2007; Bense et al. 2009).

To utilize heat as a groundwater flow tracer requires permeabilities that are sufficiently high to allow advective heat transfer. Suggested values of minimum permeabilities span the range of $5\times10^{-17}<k_{\min}<10^{-15}$ m^2 (Smith and Chapman 1983; Forster and Smith 1989; Manning and Ingebritsen 1999). Permeabilities below $k_{\min}$ tend to cause heat-conduction-dominated systems, precluding inversion of temperature fields for groundwater flow patterns and rates as well as constraint of permeabilities other than being less than $k_{\min}$. As discussed in this review, exact values of $k_{\min}$ depend on several other parameters such as the aspect ratio of the flow domain (basin depth to width), whether any high- or low-permeability faults or other heterogeneities are present, anisotropy of hydraulic and thermal parameters, background heat flow rates, and the shape of the water table. However, the range of possible $k_{\min}$ values is fairly narrow and located toward the lower third of geologic materials which typically exhibit permeabilities of $10^{-21}<k<10^{-7}$ m^2 (e.g., Freeze and Cherry 1979; Manning and Ingebritsen 1999; Saar and Manga 2004; Ingebritsen and Manning 2009). Therefore, a significant fraction of naturally occurring permeabilities and groundwater flow fields can be investigated by analyzing subsurface temperature fields and heat discharge at springs.

Background information on coupled heat transport and single-phase groundwater flow is provided in section Background. Section Geotherm measurements discusses techniques of measuring geothermal gradients (geotherms), including an overview of error sources and possible corrections. Section Using geotherms to constrain groundwater flow velocity and permeability fields investigates constraint of permeabilities and/or groundwater flow velocities in steady-state and transient systems ranging from one to three spatial dimensions. The discussion of geotherms is followed by the section Using heat discharge at springs to constrain permeabilities and groundwater flow patterns and rates. Finally, section Concluding remarks and implications summarizes this review paper and provides a brief list of fields where insights into geothermal heat transfer may be used to constrain processes of interest.

Background

Geothermal heat transfer occurs everywhere on Earth, albeit at higher rates in some regions than in others. The omnipresence of geothermal heat makes it an excellent natural tracer of various geologic processes, including groundwater flow. Earth's total heat power is approximately 44 TW, for a mean heat flow rate of approximately 87 mW/m^2 (Pollack et al. 1993). Higher heat flow rates occur in tectonically and/or volcanically active regions, while lower heat flow rates are common in more geologically stable regions. Thus, the mean heat flow for the oceanic and the continental crust is 101 and 65 mW/m^2, respectively (Pollack et al. 1993). The main sources of geothermal heat are gravitational compression during Earth's formation, accretion via impacts of extraterrestrial objects, latent heat of crystallization as the outer core crystallizes to form the inner core, and radioactive decay of unstable elements (uranium, thorium, and potassium). Heat is transferred from the Earth's interior to the atmosphere by conduction, advection/convection, and radiation. Radiation can generally be neglected at typical groundwater temperatures and as the effective radiation length scales involved within Earth are small (e.g., Turcotte and Schubert 2002). The terms advection and convection are often used interchangeably in the literature and, thus, no particular distinction is made here.

The equation describing heat transfer by conduction is a structural homology to Darcy's law (Darcy 1856),

$$\mathbf{q} = -\frac{\mathbf{k}}{\mu_{\mathrm{w}}}\cdot\nabla(P+\rho_{\mathrm{w}}gz), \tag{1}$$

where $\mathbf{q}$ is the Darcy groundwater flow velocity (specific discharge), $\mathbf{k}$ is the solid's permeability, μ_{w} is the dynamic water viscosity, ρ_{w} is water density, P is pore-fluid pressure, g is Earth's (vertical) gravitational acceleration, and z is elevation above some reference datum. Heat conduction is described by the analogous Fourier's law (Fourier 1822) as

$$\mathbf{q}_{\mathbf{h_c}} = -\mathbf{K_T}\cdot\nabla T, \tag{2}$$

where $\mathbf{q}_{\mathbf{h_c}}$ is the conductive heat flow per unit cross-sectional area, $\mathbf{K_T}$ is thermal conductivity, and T is temperature. The heat conduction or diffusion equation is also a structural homology to the groundwater flow equation, which might thus be referred to as the "hydraulic head diffusion equation." While the groundwater flow equation provides the hydraulic head field over time, $h(x, y, z, t)$, the solution to the thermal-diffusion equation is the temperature field, $T(x, y, z, t)$, in three spatial dimensions, x, y, z, and over time, t:

$$\frac{\partial T}{\partial t} = \nabla\cdot\left(\frac{\mathbf{K_T}}{\rho c}\cdot\nabla T\right) + S_{\mathrm{h}}. \tag{3}$$

Here, S_{h} accounts for heat sinks or sources, ρ is material density, c is specific heat, and the product ρc is the volumetric heat capacity. Thermal diffusivity is defined as $\mathbf{D_T} = \mathbf{K_T}\rho^{-1}c^{-1}$. Thus, temperature is analogous to hydraulic head, thermal conductivity to hydraulic conductivity, volumetric heat capacity to storativity per unit aquifer thickness, and thermal diffusivity to hydraulic

 DOI 10.1007/s10040-010-0657-2

diffusivity. In hydrogeology, the groundwater flow equation is solved before Darcy's law is applied to the resultant hydraulic head field to obtain the specific discharge (i.e., Darcy velocity). Similarly, in conductive heat transfer problems, Eq. (3) is solved to obtain a temperature field before applying Fourier's law to determine heat flow direction and rate. This analogy between heat conduction and groundwater flow has allowed generations of hydrogeologists to apply analytical solutions developed for simple heat-conduction situations (e.g., Carslaw and Jaeger 1959) to simple groundwater-flow problems.

A relatively recent development is to couple groundwater and heat transfer, solving both systems of equations simultaneously to address (1) questions regarding groundwater flow and (2) questions on heat transfer based on both hydrologic and temperature data. Anderson (2005) subdivides the former approach further into one, whereby heat is used directly as a tracer to detect groundwater–surface-water interactions or fractures and one in which geotherms are used to solve for groundwater flow velocities and/or permeability distributions. The latter approach is the primary focus discussed here, in the context of large-scale groundwater flow (see section Using geotherms to constrain groundwater flow velocity and permeability fields) although discharge of heat at hot springs (see section Using heat discharge at springs to constrain permeabilities and groundwater flow patterns and rates) is also mentioned, as it can be sensitive to large-scale flow patterns and rates.

Coupling groundwater and heat transfer, both in trial-and-error forward or in formal inverse methods (e.g., Woodbury et al. 1987; Woodbury and Smith 1988; Rath et al. 2006), requires a mathematical formulation for heat transfer that includes both heat conduction (Eq. 3) through the water-solid complex and heat advection. Heat transfer by advection occurs when fluid molecules with a given temperature move into a region with lower ambient temperatures.

A temperature-based equation describing three-dimensional conductive and advective heat transfer in a porous medium can be written as

$$\frac{\partial}{\partial t}(\phi_{\mathrm{w}}\rho_{\mathrm{w}}c_{\mathrm{w}}T+\phi_{\mathrm{s}}\rho_{\mathrm{s}}c_{\mathrm{s}}T)=\nabla\cdot\left[\frac{\rho_{\mathrm{w}}c_{\mathrm{w}}T}{\mu_{\mathrm{w}}}\mathbf{k}\cdot\nabla(P+\rho_{\mathrm{w}}gz)\right]+\nabla\cdot(\mathbf{K}_{\mathbf{T_m}}\cdot\nabla T)+S_{\mathrm{h}}, \quad (4)$$

where ϕ is a volume fraction (all other parameters are as before) and subscripts w, s, and m denote water, solid, and mixed water-solid properties, respectively. Solid and water volume fractions sum to the total volume ($\phi_{\mathrm{s}}+\phi_{\mathrm{w}}=1$) in a system that contains only one fluid phase, as mainly considered here, where geothermal heat serves as a tracer but does not cause fluid phase transitions. Modeling of multiphase, multicomponent hydrothermal systems that are influenced by magma bodies is reviewed in Ingebritsen et al. (2010). For small ϕ_{w}, mixed properties of the water-solid complex in porous media are often approximated by the linear relationship $\xi_{\mathrm{m}}=\phi_{\mathrm{w}}\xi_{\mathrm{w}}+\phi_{\mathrm{s}}\xi_{\mathrm{s}}$, where ξ represents the solid or water property of interest (e.g., Smith and Chapman 1983; Taniguchi 1993; Saar and Manga 2004). Alternative mixed property relations are also widely used, in particular the geometric mean approximation, $\xi_{\mathrm{m}}=\xi_{\mathrm{w}}^{\phi_{\mathrm{w}}}\xi_{\mathrm{s}}^{\phi_{\mathrm{s}}}$, for parameters such as thermal conductivity (e.g., Sass et al. 1971; Garven and Freeze 1984a; Walsh and Saar 2010). In Eq. (4), local thermal equilibrium between the solid and fluid phases is assumed.

As mentioned before, dividing a material's thermal conductivity by its volumetric heat capacity results in $\mathbf{D}_{\mathbf{T_m}}=\mathbf{K}_{\mathbf{T_m}}\rho_{\mathrm{m}}^{-1}c_{\mathrm{m}}^{-1}$, now expressed for mixed water-solid properties as indicated by the subscript m. In addition to thermal diffusion, mechanical heat dispersion, $\mathbf{D_{TM}}$, may also require consideration, resulting in the thermal hydrodynamic dispersion tensor, $\mathbf{D_{TH}}$. Mechanical heat dispersion is theoretically a second-rank tensor, given by

$$\mathbf{D_{TM}}=\alpha_{\mathrm{T}}\sqrt{\mathbf{q}\cdot\mathbf{q}}\,\mathbf{I}+(\alpha_{\mathrm{L}}-\alpha_{\mathrm{T}})\frac{\mathbf{q}\otimes\mathbf{q}}{\sqrt{\mathbf{q}\cdot\mathbf{q}}}, \quad (5)$$

where α_{L} and α_{T} are the longitudinal and transverse dispersion coefficients, respectively, and $\mathbf{I}$ is the identity matrix (Bear 1979). As in solute transport, α_{L} is typically much larger than α_{T} (e.g., Perkins and Johnston 1963) and thus $\mathbf{D_{TM}}$ is anisotropic even if subsurface material properties are homogeneous and isotropic. For example, Forster and Smith (1989) used α_{L}=100 m and α_{T}=10 m for heat transport. Unless the thermal conductivity of the solid is anisotropic, or anisotropic (water-filled) pore-space geometries exist, mixed thermal diffusivities of the water-solid complex are likely isotropic, i.e., $\mathbf{D}_{\mathbf{T_m}}=D_{\mathrm{T_m}}\mathbf{I}$, in which case $\mathbf{D}_{\mathbf{TH_m}}=\mathbf{D_{TM}}+D_{\mathrm{T_m}}\mathbf{I}$. To keep the notation simple, only the diffusive term, $\mathbf{D}_{\mathbf{T_m}}$, will be reported hereafter. Further, although thermal diffusivity and dispersivity (like the analogous hydraulic properties) are technically tensors, for practical purposes only one or two elements of the hypothetical tensors are generally considered.

The first term on the right-hand side of Eq. (4) describes advective heat transfer due to a Darcy (specific discharge) fluid-flow velocity vector (Eq. 1), which is multiplied by $\rho_{\mathrm{w}}c_{\mathrm{w}}T$ to account for heat energy transfer by the movement of fluid mass through the porous medium. Assuming spatially constant $\rho_{\mathrm{w}}c_{\mathrm{w}}$, applying the linear expression for mixed water-solid properties in the temporal derivative, and applying Darcy's law (Eq. 1), reduces Eq. (4) to

$$\frac{\partial(\rho_{\mathrm{m}}c_{\mathrm{m}}T)}{\partial t}=-\rho_{\mathrm{w}}c_{\mathrm{w}}\nabla\cdot(\mathbf{q}T)+\nabla\cdot(\mathbf{K}_{\mathbf{T_m}}\cdot\nabla T)+S_{\mathrm{h}}. \quad (6)$$

It should be noted that, if incompressibility of water is assumed, i.e., $\nabla\cdot\mathbf{q}=0$, then $\nabla\cdot(\mathbf{q}T)=T(\nabla\cdot\mathbf{q})+\mathbf{q}\cdot\nabla T$ reduces to $\mathbf{q}\cdot\nabla T$ in Eq. (6). In this case, however, buoyancy-driven fluid flow is not described by the

 DOI 10.1007/s10040-010-0657-2

equation, unless the Boussinesq approximation is invoked, providing non-zero $\mathbf{q}$ (in $\mathbf{q} \cdot \nabla T$) as a result of (temperature-induced) water-density inversions. Furthermore, under the incompressibility assumption, the vector dot product, $\mathbf{q} \cdot \nabla T$, implies that temperature variations caused by fluid flow can only occur if the vectors $\mathbf{q}$ and ∇T are not perpendicular. This has significant implications for using geotherms to invert for groundwater flow velocities, as discussed further in section Using geotherms to constrain groundwater flow velocity and permeability fields.

The second term on the right-hand side of Eq. (6) describes heat transfer by conduction through the water-solid complex. If it is assumed that the mixed thermal conductivity, $\mathbf{K}_{\mathbf{T_m}}$, is constant in space and isotropic, that $\rho_m c_m$ are constant in time, and ignoring the heat sink or source term, S_h, then Eq. (6) simplifies to

$$\frac{\partial T}{\partial t} = -\frac{\rho_w c_w}{\rho_m c_m} \nabla \cdot (\mathbf{q} T) + \mathbf{D}_{\mathbf{T_m}} \nabla^2 T, \tag{7}$$

which is identical to Eq. (1) of Anderson (2005). Suzuki (1960) and Stallman (1963) were among the first to use a steady-state version of Eq. (7), with $\nabla \cdot \mathbf{q} = 0$, to calculate water-infiltration rates and groundwater-flow velocities, respectively, from subsurface temperature data. Stallman (1963) moreover suggested that, in combination with hydraulic-head gradient data, this technique could be employed to constrain permeabilities.

For heat transfer by more than one fluid phase, it is advantageous to replace the volumetric heat capacity, ρc, terms for the various phases by enthalpy, H, and to introduce separate terms for heat energy transfer by liquid water and by steam, which requires the use of relative permeability terms for the fluid phases, as described for example in Ingebritsen et al. (2006).

Note that, particularly in large-scale geothermal systems, large water-temperature contrasts may exist between different regions. Thus, the hydraulic conductivity tensor, $\mathbf{K} = \rho_w g \mu_w^{-1} \mathbf{k}$, should remain decomposed (as done throughout this paper) into its components, as temperature fluctuations affect ρ_w and, in particular, the dynamic water viscosity, μ_w. Therefore, this paper discusses determining permeability, $\mathbf{k}$ (as opposed to hydraulic conductivity, $\mathbf{K}$). Pressure effects on viscosity can typically be neglected in groundwater applications. The effect of temperature on both dynamic water viscosity and water density is reflected in the kinematic viscosity, $\nu_w = \mu_w / \rho_w$, by (Germanovich et al. 2000)

$$\nu_w \approx \frac{0.032 \text{ Pa s } ^\circ\text{C}}{\rho_w (1 - \alpha_w T)(15.4^\circ\text{C} + T)}, \tag{8}$$

where $\alpha_w = 10^{-3} ^\circ\text{C}^{-1}$ is the coefficient of thermal expansion of water and Pa s are units of dynamic viscosity. Furthermore, salinity effects on water density and viscosity are often important in (deep) geothermal systems and are discussed in many publications (e.g., Kestin et al. 1981; Herbert et al. 1988).

Figure 1 illustrates the boundary conditions typically employed in numerical models of coupled groundwater and heat transfer. It is important, however, to implement advective heat discharge (Neumann) boundary conditions at hot springs (Forster and Smith 1989; López and Smith 1995). Otherwise, constant temperature (Dirichlet) boundary conditions, typically invoked to represent atmospheric or mean annual surface-temperature conditions, force unrealistic conductive heat transfer to atmospheric temperatures immediately at hot spring locations where heat is, in reality, advectively discharged. Assigning an advective heat discharge condition may be straightforward if the locations of hot springs, e.g., at faults (Fig. 1), are known (e.g., Forster and Smith 1989). However, without such a priori information, assigning the advective boundary condition at predetermined boundary locations amidst constant atmospheric-temperature boundary conditions can affect model outcome. In such cases, it is desirable to let the numerical model determine iteratively where, and how much, advective heat discharge is taking place at any portion of a surface boundary (López and Smith 1995).

To assess the relative importance of advective to conductive heat transfer, buoyancy-driven convection, and other thermal and fluid dynamical processes, several dimensionless numbers can be determined. For example, for an advective one-dimensional heat-energy flux, normalized per unit cross-sectional area, of

$$q_{h_a} = \rho_w c_w T q, \tag{9}$$

and a parallel conductive heat flow density, $q_{h_{cm}}$ given analogously to Eq. (2), the Nusselt number,

$$\text{Nu} = (q_{h_a} + q_{h_{cm}}) / q_{h_{cm}}, \tag{10}$$

represents the ratio of total (advective and conductive) to conductive heat energy transfer. If no advective heat transfer occurs, then Nu = 1. Nu depends on both fluid and solid properties, as heat is advected by the fluid and conducted through both the fluid and the solid phase.

The Peclet number is the ratio of (thermal) advection, which scales with some characteristic (scalar) Darcy velocity, q, along some characteristic length, L, to characteristic (scalar, thermal) hydrodynamic dispersion of the solid-water complex,

$$\text{Pe} = qL / D_{\text{TH}_m}. \tag{11}$$

Therefore, Pe is zero if there is no fluid flow.

The Rayleigh number,

$$\text{Ra} = \frac{\rho_r \alpha_w \Delta T \, \rho_w c_w g k L}{\mu_w K_{T_m}}, \tag{12}$$

serves to estimate the onset of convection (at high Ra), where ρ_r is the reference density of water at a reference temperature, T_R, ΔT indicates the difference between

 DOI 10.1007/s10040-010-0657-2

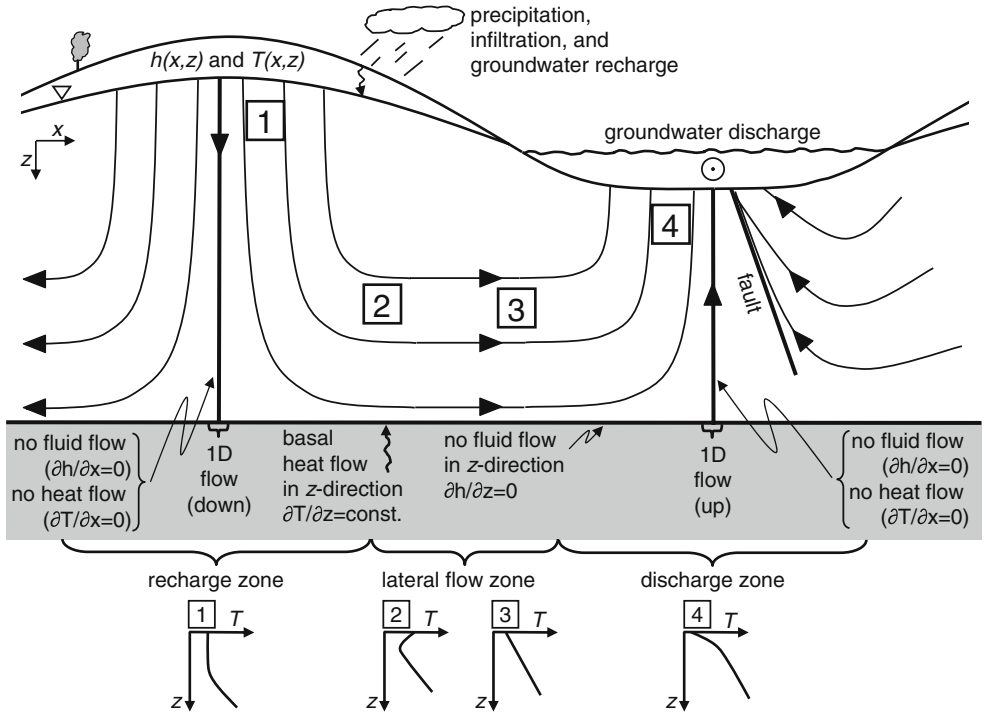

Fig. 1 Illustration of a typical (forced-convection) groundwater flow field caused by topographic relief (at any scale) that repeats horizontally and results in the indicated boundary conditions. The *bold flow lines* indicate the edges of unit flow cells where boundary conditions apply. The boundary conditions are zero groundwater and constant heat flow at the base, no heat and no groundwater flow at the sides (usually due to model symmetry representing repeated ridge-valley combinations), and constant hydraulic head and mean annual surface temperature (possibly following the adiabatic lapse rate of the atmosphere) at the *top*, representing the water table. A fault is included as a reminder that an advective heat discharge boundary condition may be required where faults outcrop as discussed in section Background. *Numbers* indicate typical steady-state geotherm profiles expected in the respective groundwater flow field regions: (*1*) isothermal (cold) near-surface profile in a recharge region, (*2*) low-temperature horizontal flow at some depth that has not completely thermally equilibrated at the given position, (*3*) linear profile as thermally equilibrated flow is perpendicular to the geothermal heat flow vector, and (*4*) elevated near-surface geothermal gradients in discharge zones.

actual water temperature and T_R, and α_w is the coefficient of thermal expansion for water. This form of Ra for porous medium convection replaces the characteristic length-cubed term, L^3, for bulk fluid convection by kL. Permeability anisotropy can also be included (Furbish 1997).

The Reynolds number,

$$\mathrm{Re} = \frac{\rho_w L}{\mu}\frac{q}{\phi_c}, \tag{13}$$

estimates the onset of turbulent (high Re) versus laminar (low Re) flow in a porous medium with connected pore fraction ϕ_c, characteristic length scale L, and seepage velocity q/ϕ_c. It is a criterion for the applicability of Darcy's law and the groundwater flow equation.

Geotherm measurements

Precise measurement of temperature as a function of depth (the geotherm) in a well is important, because even small deviations from a linear, conductive profile can represent significant advective heat transfer and indicate groundwater flow (see section Using geotherms to constrain groundwater flow velocity and permeability fields). The precise relative variation of temperature with depth is most important, the absolute accuracy of the sensors less so.

The most precise commonly employed temperature-measurement device is a thermistor (thermal resistor), which determines temperature with a resolution of ~0.001°C as a function of temperature-dependent electrical-resistivity variations in a ceramic or polymer material. However, the precision of thermistors typically decreases for T>100°C and maximum measurable temperatures tend to be at ~130°C. Resistivity temperature devices (RTDs) also measure temperature via electrical resistivity variations. They employ metals, which allows temperature measurements up to ~600°C. However, the precision of RTDs is typically lower than that of thermistors.

Relatively recently, distributed-temperature systems (DTS) have been introduced, utilizing the Raman effect to measure the temperature throughout the length of a fiber optic cable virtually instantaneously (e.g., Tyler et al. 2009). A nearly continuous temperature profile, with readings on the scale of ~1 m, can be obtained. However, DTS precision is typically lower than that of RTDs and thermal degradation of DTS can occur at high temperatures. However, ease of use and the ability to determine a geotherm within seconds facilitate collection of time-series, and thus detection of transient geotherms discussed

 DOI 10.1007/s10040-010-0657-2

in section Using geotherms to constrain groundwater flow velocity and permeability fields.

Wisian et al. (1998) provide field comparisons for several of the geotherm measurement techniques discussed in the preceding, including DTS. Wisian et al. (1998) also discuss intraborehole convection as a source of geotherm measurement errors. Generally speaking, smaller borehole diameters result in smaller Rayleigh numbers and, thus, a lower likelihood of intraborehole convection.

When interpreting advective heat transfer from geotherm measurements, so-called terrain effects may need to be taken into account. The topographic component of terrain effects result from topographic relief focusing conductive heat flow toward valleys (e.g., Birch 1950; Lachenbruch 1968). In addition, cooler atmospheric temperatures, due to the adiabatic lapse rate, at higher topographic elevations provide varying mean annual surface temperatures when topographic relief is present. Numerical models of coupled groundwater and heat transfer already take topographic effects into account because they essentially solve the conductive component of heat transfer, with its topographic effects, implicitly. In other words, if one assigns a zero permeability to the model, it reverts to purely conductive heat transfer, showing the topographic effect. Aside from standard topographic terrain effects, microclimate can affect near-surface isotherms, so that topography-parallel isotherms may not be a valid assumption (Blackwell et al. 1980). Similarly, urbanization (e.g., Ferguson and Woodbury 2007) and forest clearing or other land-use changes (e.g., Ferguson and Beltrami 2006; Bense and Beltrami 2007) can influence isotherms (e.g., Taniguchi et al. 1999a, b). Geotherms can also be affected by orogeny, lithospheric extension, erosion (causing exhumation), or burial by sediments that modify the topography and/or burial depths (e.g., Buck et al. 1988; Blythe and Kleinspehn 1998; Zeitler et al. 2001).

Heterogeneity and anisotropy in thermal conductivity, $\mathbf{K}_{\mathbf{T}_m}$, can cause non-vertical geothermal heat flow patterns. $\mathbf{K}_{\mathbf{T}_m}$ anisotropy can occur when aligned minerals cause anisotropic heat conduction properties or when pore-space geometries are anisotropic, resulting in preferred heat-flow directions. Heterogeneity can cause refraction of heat flow lines at boundaries separating different $\mathbf{K}_{\mathbf{T}}$ values. Deviations from vertical conductive heat flow can also occur when the heat source cannot be approximated by a horizontal heat source plane at depth (i.e., as a constant-temperature or constant-vertical-heat-flux boundary condition). For example, a magma intrusion (e.g., Hildreth 2007) or radiogenic heat production from locally abundant radioactive minerals (e.g., Rye and Roy 1978) can result in conductive heat transfer in all directions away from the heat source.

Diurnal and seasonal variations in atmospheric (and thus ground surface) temperature also affect subsurface temperatures and geotherms, though usually only to a maximum depth of a few meters and a few tens of meters, respectively (e.g., Pollack and Huang 2000; Smerdon et al. 2003). Seasonal effects also include snow and ice cover, which tends to insulate the surface from colder atmospheric temperatures (Pollack et al. 2005). However, melting of snow/ice can cause infiltration of cold water into the subsurface, which also affects geotherms. Furthermore, groundwater recharge can trigger earthquakes (e.g., Saar and Manga 2003) that can in turn modify fracture permeability, possibly leading to increased recharge, or to discharge of heated groundwater. It appears that such hydroseismicity is fairly common in geothermally active regions (Christiansen et al. 2005).

Climate variability can also affect geotherm profiles (e.g., Taniguchi et al. 1999a; Pollack and Huang 2000; Beltrami et al. 2005; Ferguson et al. 2006), in this case to maximum depths of ~500 m. Climate variations have much longer periods than seasonal variations and the crust effectively acts as a low-pass-frequency filter of surface temperature signals (Pollack and Huang 2000). This principle has been used to infer past climate temperatures from geotherms (e.g., Lachenbruch and Marshall 1986; Pollack and Huang 2000; Beltrami et al. 2005; Ferguson et al. 2006). Climate change influences not only mean annual atmospheric temperatures but also mean annual snow and ice coverage which, as in the seasonal case, can affect subsurface temperature profiles via insulation and through groundwater recharge during melting periods. Similarly, thawing of permafrost soil can affect geotherms and permeability fields (e.g., McKenzie et al. 2007; Walvoord and Striegl 2007; Bense et al. 2009). Furthermore, glacial coverage may reduce or eliminate local groundwater recharge, thereby reducing the elevation of the water table (Hurwitz et al. 2003b) and impacting subsurface temperature fields.

Naturally varying mechanical stresses have been shown to induce short-term periodic fluctuations in groundwater flow, particularly in geyser systems but also in aquifers in general (e.g., Rinehart 1972; Hsieh et al. 1988; Ingebritsen et al. 2006). Work by Bredehoeft (1967) revealed that solid Earth tides can affect an aquifer's specific storage, causing variations in the water levels in wells. Rinehart (1972) correlated the interval between geyser eruptions with barometric pressure variations and tidal cycles at three United States geysers with long time-series (Old Faithful and Riverside of Yellowstone, Wyoming, and Old Faithful of California). Such observations lead naturally to the question of whether naturally varying mechanical stresses can induce periodic temperature fluctuations in deep geotherms. Recently, Cermaka et al. (2009) identified tidal component periodicities in the temperature time-series collected from a borehole in Mexico. Exempting surface temperature and pressure effects upon data collection equipment, the most likely cause of such periodicities are barometric pressure and tidal fluctuations.

Precipitation infiltration and groundwater recharge can affect subsurface thermal regimes dramatically, mainly through advective heat transfer but also by modification of the water-table location; water-table location can influence the groundwater flow field and thus advective heat transfer (Smith and Chapman 1985; Forster and Smith 1989). Groundwater recharge depends on many factors including

 DOI 10.1007/s10040-010-0657-2

geographic location and local weather as well as seasonal and climate patterns. Topography affects where precipitation occurs and, together with geology, how precipitation is partitioned into overland flow, surface storage, and infiltration. Vadose zone characteristics may also be important.

Depending on the objectives of the study, several of the effects discussed in this section may need to be considered when analyzing geotherm profiles to invert for groundwater flow velocity. Some effects may be negligible or accounted for implicitly, as is the case for the topography component of the terrain effect in numerical models. However, awareness of the processes potentially affecting geotherms, independent of the large-scale groundwater flow of interest, is critical when constructing models and interpreting modeled or measured geotherms. Such efforts may be worthwhile, however, because temperature measurements are relatively easy, fast, and economical to conduct and temperatures are highly sensitive to groundwater flow. Furthermore, because thermal conductivity, specific heat, and density of the water-solid complex vary much less than porous medium permeabilities (e.g., Freeze and Cherry 1979), it is commonly stated (e.g., McCord et al. 1992; Anderson 2005) that temperature-based permeability estimates are likely more accurate, at least over large scales, than those determined on a purely hydraulic basis.

Using geotherms to constrain groundwater flow velocity and permeability fields

The objective of this paper is to discuss the use of temperature-depth (geotherm) profiles to constrain groundwater flow velocities and/or permeability fields at a large scale. Steady-state geotherms are discussed first, followed by transient geotherms.

Numerical methods typically must be employed to determine the effective permeability of a geologic formation, or of several formations, on a large (regional) scale. This requires determination of the groundwater flow (Darcy) velocity field, $\mathbf{q}$, and hydraulic head gradients, ∇h, to solve for permeability, $\mathbf{k}$, using Darcy's law (Eq. 1), keeping in mind temperature effects on kinematic viscosity (Eq. 8) and the requirement that flow is laminar, i.e., low Reynolds numbers prevail (Eq. 13). Hydraulic testing yields permeability estimates over much smaller spatial scales than numerical models, although if many such pumping tests are employed, larger-scale permeability distributions can sometimes be inferred. Core testing (e.g., Saar and Manga 1999) for permeability results in even smaller-scale permeability estimates but may be of interest to investigate local groundwater flow. It has been generally recognized that a permeability scale effect or sampling bias exists, with smaller-scale permeability tests commonly yielding lower permeabilities, while larger-scale permeabilities are typically estimated to be larger (e.g., Sánchez-Vila et al. 1996; Hyun et al. 2002), probably due to the inclusion of larger-scale high-permeability features. However, counter-examples exist—e.g., see discussion for Deming (1993) in the following and Hsieh (1998).

Steady-state geotherms

This section is subdivided into one-dimensional (1D), two-dimensional (2D), and three-dimensional (3D) model cases. The time dimension is discussed in section Transient geotherms.

One-dimensional flow

Groundwater flow velocities and hydraulic head gradients must be known to determine permeability fields. Of course groundwater flow velocities, in and of themselves, are often of interest as well. Here, four cases of 1D flow are distinguished.

First, geotherm departures from a linear profile can frequently be used to constrain vertical groundwater flow rates. The vector dot product $\mathbf{q} \cdot \nabla T$, present as a component of $\nabla \cdot (\mathbf{q}T)$ in previous equations, shows that any groundwater flow-velocity component parallel to the temperature gradient, ∇T, causes bending of the otherwise linear geotherm profile predicted by Fourier's law. As $\mathbf{q} \perp \nabla T = 0$ in $\mathbf{q} \cdot \nabla T$ and as geothermal heat flow occurs typically in a vertical direction (i.e., $\nabla T \approx \partial T/\partial z$), this usually restricts the method for resolving vertical groundwater flow components (profiles 1 and 4 in Fig. 1). More rarely, temperature gradients also exhibit an obvious horizontal (x) component (i.e., $\partial T/\partial x \neq 0$). Thus, McCord et al. (1992) were able to use advective disturbances in horizontal temperature gradients to infer horizontal groundwater-flow rates and related permeabilities on a regional scale in the San Juan Basin, Colorado-New Mexico. Their estimates were several orders of magnitude larger than those determined by hydraulic tests on a smaller scale. An alternative approach, focusing on lateral flow within semiconfining units, is presented by Lu and Ge (1996), following the classic technique of Bredehoeft and Papadopulos (1965) for determining vertical groundwater flow in such units.

Case two involves non-vertical (often subhorizontal) flow in relatively permeable units. Horizontal groundwater-flow components can sometimes be inferred from geotherms when groundwater that is hotter or colder than the ambient temperature at a given depth passes through an aquifer or conduit (e.g., Bodvarsson et al. 1982; Ziagos and Blackwell 1986) (Fig. 2). This process distorts the otherwise continuous linear geotherm profile because the hot or cold aquifer temperature provides a boundary condition that must be met by the geotherm. Under steady-state conditions, such a profile is piece-wise linear (bold lines in Fig. 2), while transient conditions involve curvature (thin curves in Fig. 2). Groundwater can be geothermally heated in one region before entering a cooler region via lateral flow. Alternatively, cold horizontal groundwater flow may come from a significantly higher,

 DOI 10.1007/s10040-010-0657-2

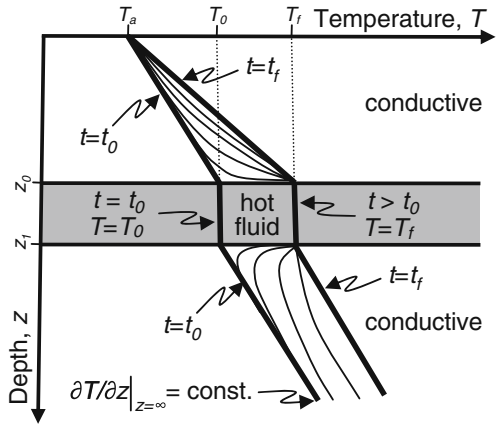

Fig. 2 Conceptual temperature versus depth (geotherm) plot illustrating steady-state (*bold lines*) versus transient (*thin curves*) geotherm profiles. Hot fluid flow in a conduit between depths $z=z_0$ and $z=z_1$ advects heat and (because water in the conduit is assumed well mixed) provides a constant temperature boundary condition which changes instantaneously from $T=T_0$ at time $t=t_0$ to $T=T_f$ immediately after t_0, i.e., at $t>t_0$. The steady-state conductive profile at the final time, $t=t_f$, is theoretically reached only at $t_f = t_\infty$ The top boundary is held at a constant atmospheric temperature, T_a, while a constant background heat flow (constant geothermal gradient) condition, $\partial T/\partial z$=constant, applies at the base of the profile.

distal recharge location with much lower mean annual surface temperature (profile 2 in Fig. 1). Groundwater flow velocities must be high enough that thermal equilibration between the water in the aquifer or conduit and the surrounding low-permeability rock is not complete (compare profiles 2 and 3 in Fig. 1). It is this non-equilibrium, but potentially steady-state (bold lines in Fig. 2) or transient (thin curves in Fig. 2), scenario that allows estimates of permeabilities and related groundwater-flow velocities in such cases.

Larger regions (relative to the conduits or aquifers of Fig. 2) can experience horizontal advective heating or cooling that is not reflected in obvious geotherm disturbances (as the whole region heats or cools). In such instances, it is useful to construct numerical models to first determine the purely conductive temperature field, which can then be subtracted from the fully coupled advective-conductive field (Forster and Smith 1989). If the resultant temperature residual is negative, advective heat transfer is extracting heat. Positive temperature residuals indicate regional advective heating.

Geotherm profile deviations from linear may also be overlooked when they are spatially limited, caused for example by narrow fracture zones. This phenomenon led Ge (1998) to propose a third geotherm perturbation case where localized lateral advective transfer of hot or cold water within a narrow fracture (zone) causes abrupt changes in the geotherm profile that are, however, only minimally affecting rock temperatures above and below the fracture.

Finally, one could argue that a fourth 1D flow case exists, namely vertical 1D flow in a recharge zone from the water table toward an impermeable layer (or with permeability decreasing to virtually zero permeability at some depth). This fourth case is discussed later prior to introduction of 2D systems.

Rearranging Eq. (7) and assuming water incompressibility, $\nabla \cdot \mathbf{q} = 0$, results in

$$\frac{\partial T}{\partial t} + \frac{\rho_w c_w}{\rho_m c_m}\mathbf{q} \cdot \nabla T = \mathbf{D}_{\mathbf{T_m}} \nabla^2 T, \tag{14}$$

illustrating that under steady-state thermal conditions, $\partial T/\partial t = 0$, the material derivative of temperature, $DT/Dt = \partial T/\partial t + \mathbf{q} \cdot \nabla T$, reduces to the advective component, $\mathbf{q} \cdot \nabla T$. Thus, vertical downwards flow of cold groundwater in a recharge region results in a concave upwards geotherm profile (see profile 1 in Fig. 1 and some profiles in Fig. 3). Conversely, regions where geothermally heated groundwater discharges are characterized by convex upwards geotherm profiles (see profile 4 in Fig. 1). In both cases, conductive heat flow is assumed to be vertically upwards, which is typically (but not always) the case. For steady-state conditions, Eq. (14) can be rewritten as

$$\mathbf{q} \cdot \nabla T = \frac{\mathbf{K}_{\mathbf{T_m}}}{\rho_w c_w} \nabla^2 T. \tag{15}$$

A classic paper, Bredehoeft and Papadopulos (1965) constrained vertical leakage through a semiconfining layer with boundaries held at constant temperature by a warm underlying confined aquifer and a cold overlaying (possibly unconfined) aquifer (Fig. 4), by solving the 1D form of Eq. (15). Casting the solution to Eq. (15) in the form of type curves that, like steady-state geotherms, bend concave upwards and convex upwards for downward and upward flow, respectively, Bredehoeft and Papadopulos (1965) provided a convenient approach for matching

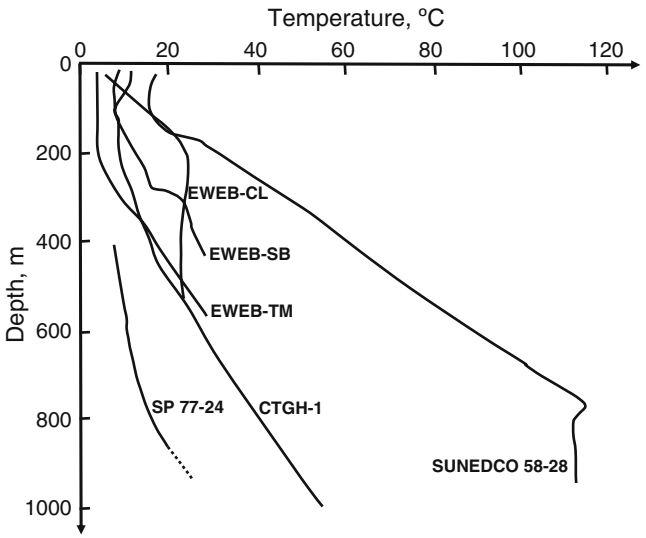

Fig. 3 Temperature-versus-depth profiles (geotherms) measured in wells. Wells labeled *EWEB-CL*, *EWEB-SB*, *EWEB-TM* were reported by Blackwell et al. (1982), data in wells *CTGH-1* and *SUNEDCO 58-28* are from Blackwell and Baker (1988), and well *SP 77-24* data are from Blackwell (1992). The wells are located in the Oregon (USA) Cascades. For precise locations, refer to the cited publications.

DOI 10.1007/s10040-010-0657-2

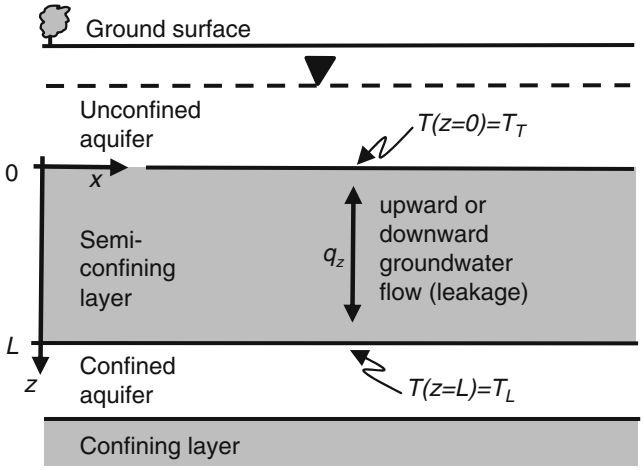

Fig. 4 Conceptual model of vertical flow or leakage (along the *z*-dimension) at a Darcy velocity, q_z, through a semi-confining layer of thickness, L, invoked by Bredehoeft and Papadopulos (1965) with constant (but unequal) top, T_T, and lower, T_L, aquifer temperatures and hydraulic heads.

temperature data from boreholes. At the same time, Stallman (1965) developed a solution for steady-state flow in a semi-infinite porous medium with sinusoidal surface-temperature fluctuations, in order to compute infiltration rates near the land surface.

By applying the Bredehoeft and Papadopulos (1965) method to the Illinois Basin (USA), Cartwright (1970) extended the approach to much larger scales, and demonstrated that it can be used to infer groundwater recharge and discharge zones that are characterized by colder and warmer temperatures than expected. The expected temperature at the depth of interest needs to be computed first, which can be non-trivial, depending on the complexity of a region's thermal processes (see section Geotherm measurements).

The method of Bredehoeft and Papadopulos (1965) was applied by Sorey (1971) to measured geotherms in the USA in the San Luis Valley, Colorado, and the Roswell Basin, New Mexico, to determine upward groundwater leakage of ~1/3 m/year through the confining beds. These values agreed well with estimates from water budgets and pumping tests. However, downward leakage rates through a clay layer near Annapolis, Maryland, were too low to be detected by the Bredehoeft and Papadopulos (1965) method.

Lu and Ge (1996) extended the method of Bredehoeft and Papadopulos (1965) to solve for the vertical temperature distribution in a semiconfining layer that experiences constant horizontal fluid and heat-flow components. Horizontal flow components within a semiconfining layer that separate an upper unconfined aquifer from a lower confined aquifer may be significant in recharge and discharge regions.

The fourth 1D flow case concerns vertical flow of groundwater and heat in a (possibly high-permeability) recharge zone. Phillips (1991) derived a solution for the geotherm in a 1D groundwater recharge region with constant mean permeability underlain by an impermeable layer (Fig. 5). This configuration results in a linear decrease in vertical groundwater flow velocity, to a value of zero at the base of the 1D flow zone. The vertical fluid- and heat-flow boundary conditions at the base are no-fluid-flow ($q_z = 0$) and constant heat flow ($q_{h_z} = -K_{T_z}\partial T/\partial z = const.$). Phillips (1991) expresses the vertical downward groundwater flow velocity as a function of the radius of curvature of the water table, $R = -\left(\partial^2 h/\partial x^2\right)^{-1}$, at $x = 0$. This formulation can be a convenient method for inverting for groundwater flow velocities if multiple spatially distributed water-table depth measurements exist, or if the water table can be assumed to be a subdued replica of the topography, allowing water-table approximation from topography. The top boundary condition is a constant hydraulic head and a constant temperature, representing for example mean annual surface temperature or atmospheric temperatures. Permeability must be estimated to invert for groundwater flow velocities or, alternatively, permeability can be solved for if measurements or estimates of the basal heat flux, heat flow/temperature boundary conditions, and R are available (Saar and Manga 2004).

The method of Phillips (1991) was modified by Saar and Manga (2004) to allow for exponentially decreasing permeability with depth. This was done because (1) permeability is expected to decrease with depth due to compaction and other processes and (2) decreasing permeability with depth results in negligible permeability values at some depth, where an impermeable boundary can be placed without significantly affecting modeling results. Because constant permeabilities result in linearly decreasing vertical groundwater-flow velocities in the recharge zone, the placement of an impermeable model boundary at an arbitrary depth directly scales all flow velocities along the vertical profile. In contrast, when permeability itself decreases with depth (linearly, exponentially, or according to a power law), then there is a negligible permeability at some depth where an impermeable model boundary can be placed without affecting flow velocities along the profile. This is particularly useful when the existence, or exact depth, of some low-permeability layer is unknown. Of course, the uncertainty regarding placement of a low-permeability layer is replaced

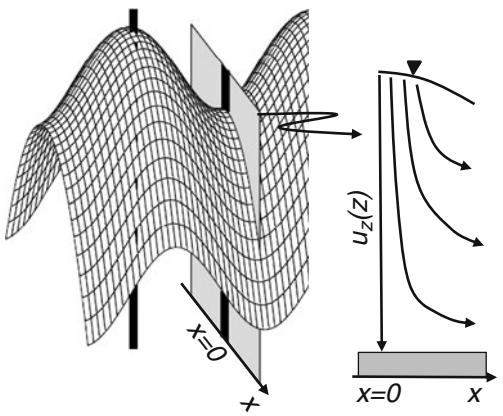

Fig. 5 Conceptual model of one-dimensional groundwater recharge along the *z*-dimension at the center ($x=0$) of a saddle between two mountains at a vertical velocity, u_z, as a function of depth, z. Modified from Saar and Manga (2004).

DOI 10.1007/s10040-010-0657-2

by uncertainty regarding how permeability should decrease with depth (Manning and Ingebritsen 1999; Saar and Manga 2004; Ingebritsen and Manning 2009). Knowledge of some model parameters such as geotherms, water-table curvatures, and groundwater recharge rates may allow constraint of unknown parameters. For example, Saar and Manga (2004) derived a semi-analytical solution to the 1D (vertical) form of Eq. (15) with an exponentially decreasing permeability profile. Employing mean annual surface (mean groundwater recharge) temperature, water-table curvature (from mean ground-surface curvature), and independently determined groundwater recharge rates, they constrain horizontal permeability and its variation with depth, as well as the background heat flux in the Oregon Cascades.

Two-dimensional systems

Several studies have investigated 2D steady-state systems of coupled groundwater and heat transfer solving Eq. (15), sometimes with the thermal diffusion coefficient, $\mathbf{K}_{\mathbf{T_m}}\,\rho_w^{-1}c_w^{-1}$, included within the divergence term, $\nabla^2 T = \nabla \cdot \nabla T$, to allow for heterogeneous and anisotropic heat conduction. These 2D analyses include the classic studies (discussed next) by Domenico and Palciauskas (1973), who investigated topography-driven (forced) heat advection in regional systems; Smith and Chapman (1983), who investigated the sensitivity of the subsurface thermal regime and surface heat flow to changes in permeability, hydraulic anisotropies and gradients, depth of the active flow field, and other aquifer properties; and Forster and Smith (1989), who studied the thermal regime of mountainous terrain with significant topographic relief of >600 m.

Domenico and Palciauskas (1973) is discussed in detail by Anderson (2005). Here, the focus is on one conclusion of that paper, namely the modification of the standard Peclet number (Eq. 11), which is usually defined for a point. Domenico and Palciauskas (1973) developed a basin-scale Peclet number, $\mathrm{Pe_b}$, which takes into account the effects of basin depth, z_0, and basin length, L_b, to characterize how much the thermal regime of an entire basin is affected by advective heat transfer. They suggest that

$$\mathrm{Pe_b} = K_H l_c (z_0/L_b)/D_{T_m}, \tag{16}$$

where $K_H = \rho_w g k/\mu_w$ is the (here scalar) hydraulic conductivity, with k representing the (here scalar) permeability, and l_c indicates some characteristic length scale. As the numerator in Eq. (16) represents the vigor of fluid flow (similar to Darcy's law) and, thus, the system's potential for heat advection, then l_c must represent some potential for driving fluid flow. Domenico and Palciauskas (1973) find that l_c is "equivalent to the mean water-table elevation and to the maximum height of the water table, both with reference to z_0, and to the amplitude of water-table oscillations." The z_0/L_b term accounts for increased advective geotherm disturbances in systems that have large height-to-width ratios, a concept addressed further by Smith and Chapman (1983) and Forster and Smith (1989).

Smith and Chapman (1983) provide an overview of the thermal effects of groundwater flow on regional-scale flow systems, with reference to 20 other papers that had been published on the topic by that time. They essentially employ Eq. (15) in two dimensions with, however, the mixed thermal diffusivity expression $\mathbf{K}_{\mathbf{T_m}}$ inside the divergence term, allowing for both heterogeneity and anisotropy in $\mathbf{K}_{\mathbf{T_m}}$. The main conclusion of their paper is that sufficiently high vertical groundwater flow velocities, caused by vertical permeabilities $>5\times10^{-17}$ m^2 (for the 40 km long and 5 km deep basin investigated), are required to cause advective effects on the thermal regime. They report that the permeability transition between conduction- and advection-dominated heat transfer is quite sharp, compared to the 13 or more orders of magnitude range of permeability exhibited by geologic materials (e.g., Freeze and Cherry 1979). Indeed, permeability threshold values of $k \approx 10^{-15}$ m^2 and $k \approx 10^{-16}$ m^2 were subsequently implied or suggested by Forster and Smith (1989) and Manning and Ingebritsen (1999), respectively, as discussed later. Smith and Chapman (1983) further conclude that vertical groundwater-flow velocity components can be reduced below the threshold values required to cause geotherm perturbations when the ratio of horizontal to vertical permeability is increased and/or, in accordance with Domenico and Palciauskas (1973), when the basin depth is reduced. In a later publication, Smith and Chapman (1985) show that the shape of the water table (linear, convex, concave) also affects the subsurface thermal regime. This implies that multiple geotherm measurements could conceivably be used to infer water-table shapes, and associated flow patterns, over large scales. Similar dependencies of fluid flow, heat transfer, and resultant subsurface temperature distributions on basin geometry, water-table configuration, and permeability distribution were also reported by Garven and Freeze (1984b) who developed a steady-state 2D model of gravity-driven (i.e., forced convective) fluid flow in a sedimentary basin (Garven and Freeze 1984a).

Forster and Smith (1989) employed a 2D, steady-state model (Fig. 6), solving Eq. (15) with $\mathbf{K}_{\mathbf{T_m}}$ inside the divergence term, that was based on their previous methods development (Forster and Smith 1988a, b). Their model included a variable water-table location, upper high-permeability and lower low-permeability zones, and a fracture discharging to a (hot) spring at the surface. They investigated the effects of surface topography (convex versus concave), infiltration rate, and permeabilities on the subsurface thermal regime and springs. They showed, for example, that advective heat transfer could cause a 200% or more overestimation of basal heat flow rates when geotherm data are collected only on valley floors with terrain permeabilities $>10^{-17}$ m^2. This overestimation is caused by heat advection extending from beneath recharge zones to the discharge zone in the valley. Forster and Smith (1989) also point out that linear geotherms suggest purely conductive heat transfer only in low-relief terrain. In high-relief terrain with only conductive heat transfer, geotherms can be non-linear due to the terrain effect mentioned in section Geotherm

 DOI 10.1007/s10040-010-0657-2

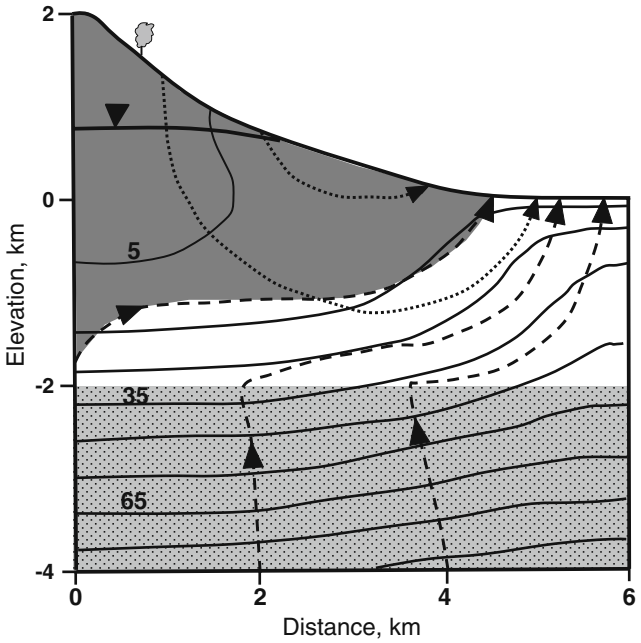

Fig. 6 Groundwater flow and thermal regime in mountainous terrain. *Thinner solid lines* indicate isotherms in °C, *dashed lines* heat flow directions, and *dotted lines* groundwater flow directions. The *bold solid line* near the surface marks the water table. The *lower gray-shaded region* is a low-permeability zone with $k=10^{-22}$ m^2. The upper of the two regions exhibits $k=10^{-15}$ m^2. The *upper gray-shaded region* indicates where basal heat flow is masked by the cold recharge. Illustration modified from Fig. 3g in Forster and Smith (1989).

measurements. Their study corroborates the finding that it is predominantly vertical groundwater flow components that affect geotherms. They go on to emphasize that high-relief and narrowly spaced ridges and valleys will increase vertical flow velocities. Therefore, geotherm perturbations by heat advection should be more common in mountainous terrain, as later also demonstrated for the Swiss Alps by Bodri and Rybach (1998), who emphasized that the reduced heat-flow regime in the recharge region (topographic high) is typically broad, while elevated heat transfer zones in valleys are narrow. Forster and Smith (1989) further show that some regions of a mountainous 2D flow regime can exhibit inverted geotherm profiles where isotherms bend from horizontal through vertical (Fig. 6). They suggest that such geotherm inversions might be expected below the flanks of mountains where the vertical relief to horizontal extent ratio is about 1/3 and permeabilities are $>10^{-15}$ m^2. These conditions allow significant groundwater recharge that can completely mask the background heat flux (e.g., Ingebritsen et al. 1992, 1993; Figs. 7 and 8) and cause such geotherm inversions. Indeed, Forster and Smith (1989) emphasize that inverted geotherms have been observed below the flanks of mountains, for example by Steele and Blackwell (1982) at Mt. Hood, Oregon. This observation suggests permeabilities of $>10^{-15}$ m^2 for the bulk volcanic complex, which agrees with vertical bulk permeability estimates for Mt. Hood specifically and the Oregon Cascades in general for depths shallower than approximately 1 km, as determined by hydrogeologic, thermal, and seismic modeling constraints

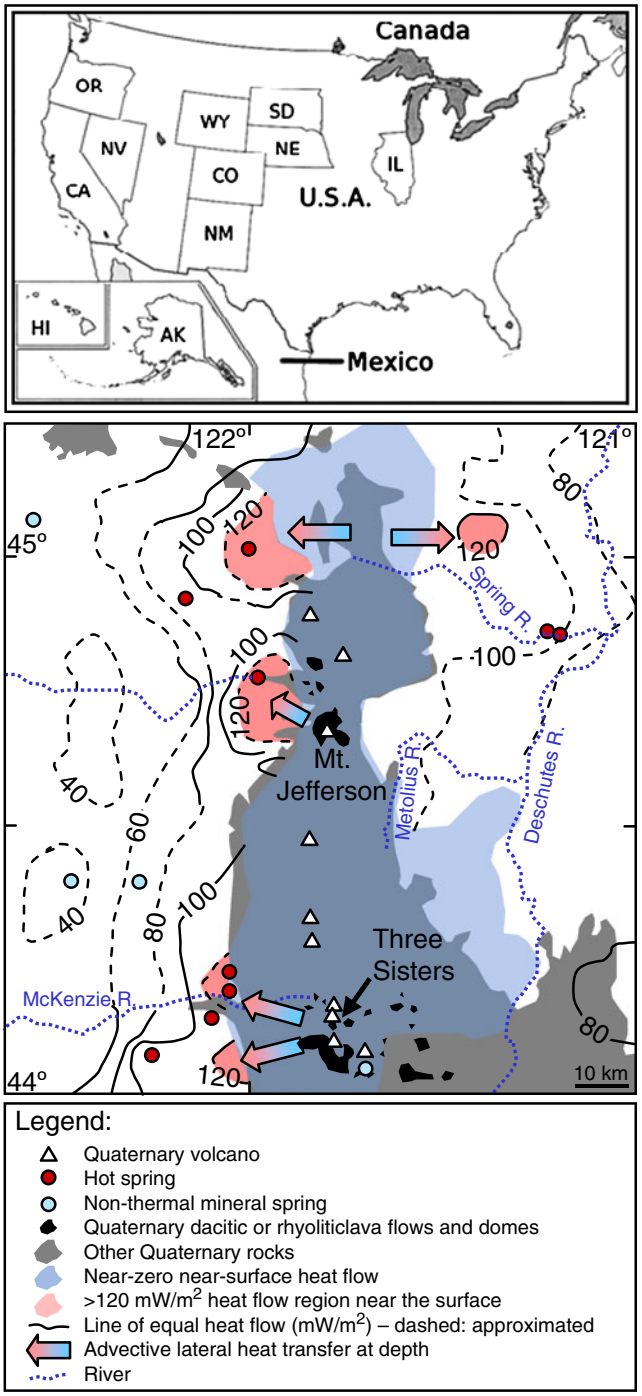

Fig. 7 Top: Map of the USA indicating the states that are mentioned in this publication, where *AK* is Alaska, *CA* California, *CO* Colorado, *HI* Hawaii, *NE* Nebraska, *NM* New Mexico, *NV* Nevada, *OR* Oregon, *SD* South Dakota, and *WY* Wyoming. *Center*: Geothermal map of a section of the Oregon Cascades. Near-zero near-surface geothermal heat flow rates in the High Cascades are caused by cold groundwater recharge that is masking elevated background heat flow rates in this volcanically active arc. Lateral groundwater flow advects the "mined" heat and discharges it at springs on the flanks of the arc as discussed in the main text. The Breitenbush Hot Springs area is the high-heat-flow area to the west of Mt. Jefferson. Modified from Ingebritsen et al. (1993). *Bottom*: Legend for center map.

DOI 10.1007/s10040-010-0657-2

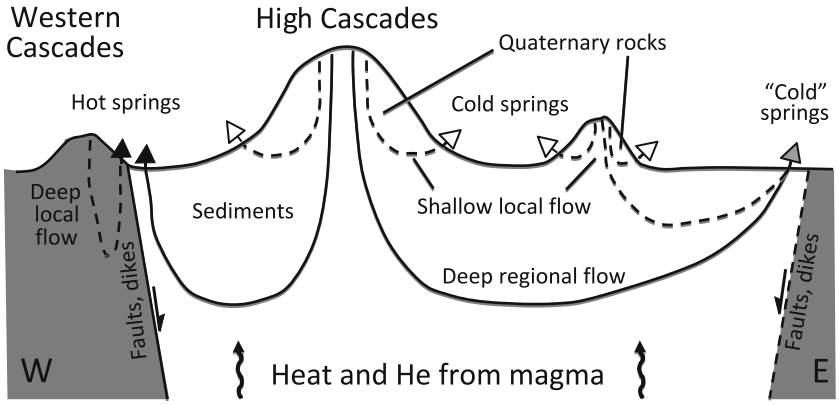

Fig. 8 Conceptual, vertically exaggerated cross section with a horizontal length of approximately 40 km through the Oregon Cascade Range. The figure illustrates that the lowermost groundwater flow path experiences the predominant influx of heat and magmatic helium (He) while shallow flow paths remain shielded from such influxes by deeper flow paths. Figure modified from Saar et al. (2005).

(Saar and Manga 2003, 2004). Such values also agree with permeability estimates for fractured igneous rock (e.g., Freeze and Cherry 1979) and with Manning and Ingebritsen (1999), who state that permeabilities $\geq 10^{-16}$ m^2 are typically required to observe advective heat transfer.

A series of publications by Ingebritsen et al. (1989, 1992, 1993, 1994) investigated rates and patterns of groundwater flow in the Oregon Cascades (Fig. 7) and their effects on subsurface temperatures. Conclusions in several of these papers are based on 2D (cross-sectional) models of coupled heat and groundwater transfer constrained by geotherms, hot spring discharge rates, and geochemical data. For example, Ingebritsen et al. (1992) conduct simulations along two cross sections in Oregon, one through the Breitenbush Hot Springs area where no major arc-parallel (and thus perpendicular to the east–west cross section) normal faulting exists, and one in the McKenzie River drainage area where major faults bound the High Cascades graben. The models are used to infer large-scale bulk permeabilities of ~10^{-14} m^2 and ~10^{-17} m^2 in the youngest and oldest rocks, respectively. High groundwater recharge rates of >1 m/year are also inferred. Furthermore, the models demonstrate that the near-surface, near-zero heat flow patterns observed in the High Cascades (Fig. 7), can be reproduced by, and thus likely stem from, cold groundwater recharge that initially flows downward—as also seen by Saar and Manga (2004)—and eventually laterally, exiting at springs on the flanks of the Cascades. During such flow, water is geothermally heated along the deepest paths, resulting in heat discharge and sometimes, but not always, hot springs, as discussed in section Using heat discharge at springs to constrain permeabilities and groundwater flow patterns and rates. Ingebritsen et al. (1992) illustrate that observed thermal patterns can be explained by significant advective heat transfer in the Breitenbush and the McKenzie River areas that mines heat from "a narrower, spottier deep heat source that is confined to the Quaternary arc and is flanked by relatively shallow conductive heat flow anomalies caused by regional groundwater flow." Therefore, according to Ingebritsen et al. (1992), an alternate model (e.g., Blackwell et al. 1982, 1990) of a laterally extensive midcrustal heat source is not required to explain the subsurface thermal structure and, in fact, appears to complicate reproduction of temperature data in the Breitenbush area. These two hypotheses regarding the spatial extent of the heat source beneath the Oregon Cascades have led to a controversy (Blackwell and Priest 1996; Ingebritsen et al. 1996) whose resolution likely requires deep drilling in high heat flow areas within the older rocks of the Western Cascades, as gravity, electrical, and magnetic data are inconclusive (Ingebritsen et al. 1992). The Oregon Cascades studies are excellent examples of how coupled groundwater and heat-flow observations and models provide insights not only into hydrogeologic processes, but also into other geologic phenomena such as the nature of the magmatic "plumbing" system beneath Cascades volcanoes (e.g., Hildreth 2007), background heat-flux rates, and geothermal energy potential.

The Oregon Cascades are predominantly an unconfined-aquifer, groundwater recharge-dominated system. Gosnold (1999) presented analytical and numerical modeling results, based on data from earlier work (Gosnold 1985, 1990), for basin-scale groundwater and heat flow in a confined-aquifer system. The confined aquifer is, however, open in its recharge and discharge regions, where temperature and heat flow results are similar to those in the recharge and discharge zones of the Cascades (Fig. 7). As some lateral flow paths in the Cascades may also be viewed as (virtually) confined, the Gosnold (1999) model may be viewed in some sense as a horizontally stretched version of the Cascades models. This system is located in south-western South Dakota and northern Nebraska (Fig. 9). The analytical solution employed is that reported by Stallman (1963), and results in downward and upward groundwater flow velocity estimates of 5×10^{-9} and 5.4×10^{-9} m/s, respectively. The 2D finite-difference model employed by Gosnold (1999) extends over a vertical distance of 2,650 m and a horizontal distance of 309 km and simulates groundwater and heat transfer through a confined aquifer extending eastward from the Black Hills of South Dakota. The numerical model includes radioactive heat production in the basement rocks. It is compared to the analytical wedge model of Jessop (1989) and found to be in good agreement. The

 DOI 10.1007/s10040-010-0657-2

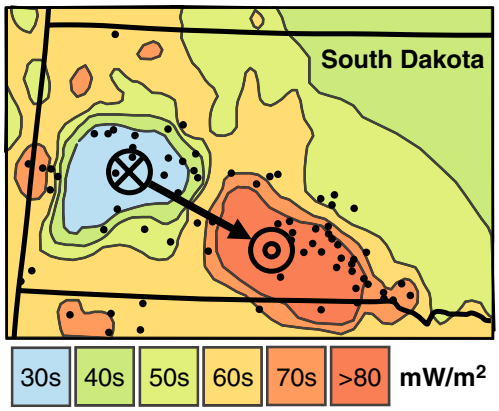

Fig. 9 Heat flow map of South Dakota, based on the map generated by Blackwell and Richards (2004), showing low near-surface geothermal heat flow rates of ~30 mW/m^2 in the Black Hills where cold groundwater recharges. The *red region* indicates high heat flow rates of >80 mW/m^2, and possibly as high as ~140 mW/m^2 (Gosnold 1999), which are likely caused by discharge of groundwater that has "mined" the heat beneath the Black Hills as discussed in the main text. *Circles* indicate approximate locations of main measurement points as presented by Blackwell and Richards (2004).

model results suggest that an elevated background (i.e., deep) geothermal heat flux rate of 91 mW/m^2 may exist beneath the aquifer recharge location in the Black Hills, due to the effects of the Laramide orogeny and mid-to-late Tertiary magmatism (Gosnold 1999). This elevated background heat flow is masked by near-surface heat-flow values that are reduced to ~30 mW/m^2 by cold groundwater recharge in the Black Hills (Fig. 9), a situation analogous to that in the Oregon Cascades. Background heat flow values are likely normal for the region (58± 9 mW/m^2) below the (confined) aquifer and outside the Black Hills region. Near-surface heat flows of close to 140 mW/m^2 in the discharge zone in eastern South Dakota (Fig. 9) are due to advective discharge of the heat "mined" in the Black Hills. This phenomenon is analogous to the heat discharge on the flanks of the Oregon Cascades. Finally, between the recharge and discharge zones, lateral advective heat transfer within the 600-m-thick confined aquifer is masked by conductive heat transfer within the overlaying confining units, which range in thickness from 2,000 m (in the west) to 500 m (in the east). Such transfer masking effects are further discussed in section Using heat discharge at springs to constrain permeabilities and groundwater flow patterns and rates. Within the lateral flow region, the system is analogous to that described by Bodvarsson et al. (1982) and others (Brott et al. 1981; Ziagos and Blackwell 1986), in which a confined (hot) aquifer serves as a boundary condition for conductive heat transfer above (and below), as illustrated in Fig. 2. The model by Gosnold (1999) suggests average horizontal groundwater flow (Darcy) velocities of 1–2 m/year within the confined aquifer.

A large regional-scale groundwater and heat transfer model was developed by Deming (1993), who ran the transient 2D finite-difference model described by Deming and Nunn (1991) to quasi-steady-state conditions to constrain the permeability field on the north slope of Alaska. The model extends 330 km horizontally and up to 12 km vertically, from the Brooks Range in the south to the Arctic Ocean in the north, and consists of 9 units. Within each unit, permeability and thermal conductivity are homogeneous, but permeability could be anisotropic. Model boundary conditions are essentially as given in Fig. 1, albeit, with constant hydraulic head (instead of no-fluid-flow) conditions on the right-side (north) boundary, to represent the ocean, and portions of the top boundary impermeable to groundwater recharge, reflecting permafrost conditions. Both topography- and buoyancy-driven flow were considered. The model was constrained by near-surface heat flow measurements projected onto the cross section, rather than geotherms, because the model errors in temperatures are larger (particularly at greater depths) than errors in heat flow. The model also included internal radiogenic heat production, and background heat flow rates at its base were adjusted to yield a constant near-surface heat flow of 50 mW/m^2 in the conduction-only basecase. Deming (1993) found that effective horizontal and vertical basin-scale permeabilities are $2.5 \times 10^{-14} \leq k_x \leq 2.5 \times 10^{-13}$ m^2 and $1.0 \times 10^{-16} \leq k_z \leq 5.0 \times 10^{-16}$ m^2, respectively, and thus estimated that permeability anisotropies, k_x/k_z, range from 100 to 1,000. The modeled average effective horizontal permeability agrees reasonably well with an arithmetic mean permeability of 6.1×10^{-14} m^2 measured on 2,031 cores (Deming 1993). Thus, permeability scale effects do not appear to be present, or are at least not pronounced, in this study region.

A very deep 2D (15 km deep and 35 km wide), quasi-steady-state model of coupled groundwater, heat, and solute (isotope) transport was developed by Person et al. (2007) to investigate the hydrologic and thermal controls on fluid–rock isotope exchange in metamorphic core complexes. Assuming a basal heat flux of 90 mW/m^2, they found that heat and isotope signatures inferred from samples of the Shuswap core complex in British Columbia, Canada, require fault permeabilities of $10^{-16} < k \leq 10^{-15}$ m^2 to allow sufficient circulation of meteoric waters. The country rock permeability is constrained to be $<10^{-17}$ m^2. Similarly, Person et al. (2008) found field evidence for deep fluid circulation and convection in modern and fossil geothermal systems in the Great Basin. They employed a suite of 2D local (~45 km) to regional (~100 km) scale models and deduced that anisotropic, subvertical faults are frequently connected by permeable aquifers at depth, allowing convection patterns to form. Modern geothermal systems in the Great Basin were also investigated by Coolbaugh et al. (2005) who reported that deep fractures and normal faults, caused by the active tectonic extension in this region, result in the circulation and heating of meteoric fluids and formation of hydrothermal systems. Fault-dominated systems are discussed further in following sections.

Three-dimensional systems

The 3D characteristics of coupled groundwater and heat transfer are less frequently explored than 1D or 2D flow. In many special cases, 1D groundwater and

DOI 10.1007/s10040-010-0657-2

heat flow may fully describe a particular process of interest. Similarly, some conceptual model geometries are intrinsically 2D such as a ridge-basin system, unless variations along the ridge axis are important. However, some problems require quasi-3D or fully 3D treatment, sometimes with consideration for the time dimension as discussed in the next section. The third spatial dimension is important, when significant variations (e.g., changes in permeability, groundwater recharge, water-table elevation, thermal conductivity, background heat flux) occur along that dimension. For instance, Ingebritsen et al. (1992) found that their two-dimensional simulations cannot simultaneously match some geotherm and near-surface heat flow data.

Sorey (1976) and Sorey et al. (1978) present a 3D, transient, integrated-finite-difference model for Long Valley Caldera (LVC), California, employing a version of Eq. (6) without a sink/source term, with temporally constant $\rho_m c_m$, and with $\nabla \cdot \mathbf{q}=0$, resulting in

$$\rho_m c_m \frac{\partial T}{\partial t} = -\rho_w c_w \mathbf{q} \cdot \nabla T + \nabla \cdot (\mathbf{D}_{\mathbf{T}_m} \nabla T). \quad (17)$$

Both the overall caldera shape (elliptical) and the heterogeneity of the caldera (rim and interior topography, differing groundwater recharge rates along the rim, northwest-trending fault zone) preclude the use of a 2D or radially symmetric model for the entire region. The model is partially constrained by the combined advective and conductive heat discharge of the caldera which Sorey (1976) and Sorey et al. (1978) estimate to be 3×10^8 W. It consists of five horizontal layers spanning a total depth of ~6 km. Groundwater recharge to the upper model layer occurs along the western and north-eastern sections of the caldera ring fault, as suggested by isotope data, water-table elevations, and cold, isothermal geotherms (as by profile 1 in Fig. 1 and several profiles in Fig. 3). Geotherms in the interior of the caldera are used to constrain the model, along with other hydrologic data such as the discharge at Hot Creek Gorge (as hot springs within the creek), which ranges from 190 to 300 kg/s. Additional groundwater discharge is hypothesized, and modeled, underneath the southeast rim. The three models developed consider a hydrothermal system with (1) a uniform reservoir permeability distribution, (2) a fault-zone permeability distribution, representing the northwest-trending fault zone running through the center of the caldera, and (3) a low-permeability-block (at Casa Diablo) reservoir-permeability distribution. The models provide estimates for the permeability structure which are then compared with laboratory permeability measurements on cores taken from the caldera. The three numerical models result in an estimated permeability range of $3\times10^{-14}\leq k\leq3.5\times10^{-13}$ m^2, agreeing fairly well with LVC core measurements of $1.8\times10^{-13}\leq k\leq5\times10^{-11}$ m^2. The fault-zone model requires significantly deeper fluid circulation depths (to reach required reservoir temperatures of >200°C) than the other models.

Woodbury and Smith (1985) built upon the 2D model developed by Smith and Chapman (1983). They solved Eq. (15) numerically, with $\mathbf{K}_{\mathbf{T}_m}$ inside the divergence term, $\nabla^2=\nabla\cdot\nabla$, to allow for heterogeneity and anisotropy in $\mathbf{K}_{\mathbf{T}_m}$, to investigate the effects of 3D groundwater flow on the subsurface thermal regime. They found that water-table variations transverse to the main, regional water-table gradient can significantly affect the subsurface thermal regime and the inferred background heat flux. They stated that the exact magnitude of the disturbance depends on the "interplay of the three-dimensional water-table configuration, basin geometry including the depth to the basal impermeable boundary, anisotropy, and permeability of the subsurface formation." This again implies that hydrologic parameters, groundwater flow patterns, and depths and extent of groundwater recharge and discharge regions may be inferred from subsurface temperature measurements.

The interplay between country rock hydrology and a fault is often a 3D problem. López and Smith (1995) investigated numerically fluid and heat transfer patterns resulting from the interactions of forced, topography-driven groundwater flow through country rock and thermally driven convection in a steeply dipping fault (Fig. 10a). They found that in a diagram of country rock versus fault permeability, four fields

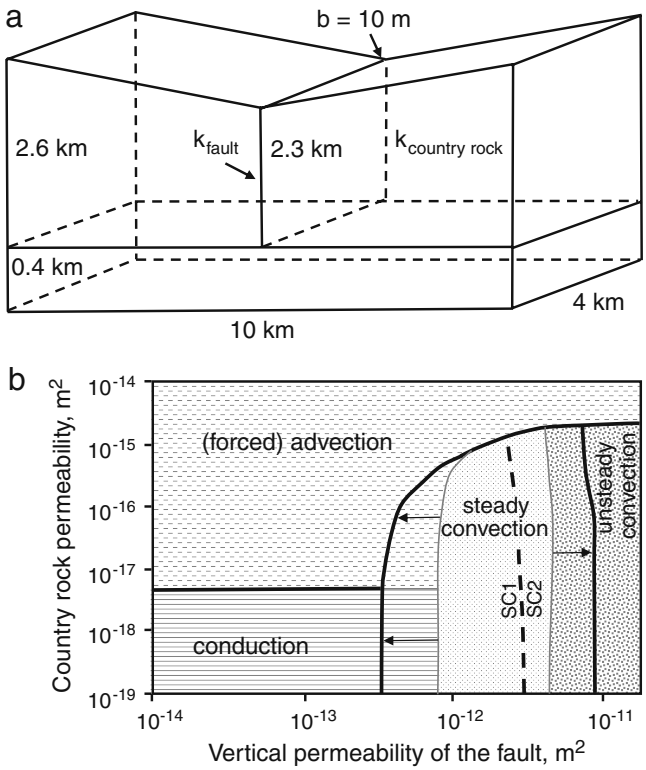

Fig. 10 **a** Model domain invoked by López and Smith (1995) and López and Smith (1996) with a basal heat flow of 90 mW/m^2 and a basement permeability of 10^{-22} m^2 (*lower box*). **b** Thermal regimes for isotropic fault permeabilities (pattern-filled fields) and a horizontal to vertical fault permeability ratio of 4 (*bold lines*) showing expansion (*arrows*) of the steady convection regime along the fault permeability axis in the anisotropic permeability case. For the given model geometry and boundary conditions, the *dashed line* separates steady convection regimes with one (*SC1*) and two (*SC2*) convection cells in the anisotropic fault permeability model. Both figure panels are modified from López and Smith (1995) and López and Smith (1996).

DOI 10.1007/s10040-010-0657-2

of fluid flow and heat transfer regimes can be distinguished: conductive, (forced) advective, steady convective, and unsteady convective (Fig. 10b). They showed that for country rock and fault permeabilities of $<5\times10^{-18}$ m^2 and $<7\times10^{-13}$ m^2, respectively, conduction dominates the entire system while buoyancy-driven convection within the fault dominates for country rock and fault permeabilities of $<2\times10^{-15}$ and $>7\times10^{-13}$ m^2, respectively. For all other permeability combinations, they suggested that forced advective heat transfer is dominant. They also stated that convective systems with country rock permeabilities $<2\times10^{-17}$ m^2 exhibit water circulation predominantly within the fault and little interaction with country rock fluids. Several other interesting conclusions concern the influence of country rock versus fault permeabilities on advective heat transfer and heat discharge at hot springs. Finally, effects of basal heat flow, thermal conductivity, as well as fault depth and length on the four fluid flow and heat transfer regimes were also discussed.

In a subsequent paper, López and Smith (1996) studied the influence of hydraulic anisotropy and heterogeneity on the four fluid flow and heat transfer regimes. They found that horizontal to vertical fault permeability ratios of 4–10 expand the steady convection field along the fault permeability axis in Fig. 10b. Conversely, if the permeability ratio for horizontal to vertical fault permeability is inverted, then lower country rock permeabilities than in the isotropic-fault-permeability case are able to suppress buoyancy-driven convection in the fault. Finally, López and Smith (1996) reported that permeability heterogeneity within the fault causes channeling of fluid flow as well as spatial variations in geotherms.

Thermal anomalies due to preferential flow along faults within unconsolidated sedimentary aquifers were also observed by Bense et al. (2008) who collected geothermal data in approximately 20 piezometer nests installed in boreholes along the Rurrand Fault in the Lower Rhine Embayment in Germany. They employed a finite-element code to solve Eq. (7) and found that the fault behaves as a conduit-barrier system as proposed by Bense and Person (2006). Such conduit-barrier systems allow preferential fluid flow along the fault while across-fault permeabilities and related flow are relatively reduced allowing significant hydraulic head gradients across the fault to be maintained, as observed in many field settings.

Preferential flow paths along faults were also investigated by Fairley and Hinds (2004) who developed a geostatistical geotherm model that was based on over 700 ground and spring temperature measurements along a 1-km section of the Borax Lake Fault in south-eastern Oregon. The composite geothermal model of a 2D horizontal plane at the surface was based on 100 simulations and used to constrain a vertical, analytical 1D heat-convection-diffusion model. They found the high-permeability flow paths within the fault transport to be a significantly higher flux than that of an average flow path but that the small areal extent of fast flow paths results in a negligible integrated contribution of all fast flow paths compared to the total fault-parallel flux.

Three-dimensionality may even be required, when no material heterogeneities or water-table variations are invoked in the third dimension, however, the flow field diverges along the third dimension. This is the case during radially symmetric flow, during which flow lines diverge in the third dimension as radial distance, r, from the central axis increases. Therefore, radially symmetric flow is here considered a form of 3D flow, even though only r and the vertical dimension, z, are modeled. For example, assuming radial symmetry for Mt. Hood, Oregon, Saar and Manga (2004) use the steady-state Eq. (15) in a cylindrical coordinate system,

$$q_{\mathrm{r}}\frac{\partial T}{\partial \mathrm{r}}+q_{\mathrm{z}}\frac{\partial T}{\partial \mathrm{z}}=\frac{K_{T_{\mathrm{m}}}}{\rho_{\mathrm{m}}c_{\mathrm{m}}}\left(\frac{\partial^2 T}{\partial \mathrm{r}^2}+\frac{1}{r}\frac{\partial^2 T}{\partial \mathrm{z}^2}\right). \tag{18}$$

The $1/r$ term in Eq. (18) accounts for the diverging heat-conduction field as r increases. The underlying groundwater flow equation also needs to be solved in cylindrical coordinates so that the Darcy velocities, q_{r} and q_z in Eq. (18), account for the radially diverging groundwater flow field. Furthermore, the model has constant heat flow and zero groundwater flow conditions at the base, zero fluid and heat flow boundaries at the cylinder center (due to symmetry) and at a specified radial distance where discharge likely occurs, and constant hydraulic head and temperature boundary conditions at the top. Saar and Manga (2004) compare model results to geotherm measurements in three boreholes and to hydrologic data (Ingebritsen et al. 1994) and suggest that the horizontal near-surface hydraulic conductivity at Mt. Hood, constrained to be $K_{\mathrm{h}} = 10^{-6}$ m/s ($\sim k = 10^{-13}$ m^2) by the model, decreases exponentially with a skin depth of $\delta=$ 250 m. Minimizing model and measurement misfits also suggests that vertical hydraulic conductivities and permeabilities are reduced by a factor of approximately 30 with respect to these parameters in the horizontal direction, that groundwater recharge velocities are ~1 m/year, and that the background heat flow is approximately 134 mW/m^2. Therefore, this coupled groundwater and heat transfer model considers both anisotropy and depth-dependence of hydrologic parameters. Furthermore, the model provides, via estimates of groundwater flow velocities and the skin-depth parameter for the rate at which permeability decreases with depth, a means for estimating maximum depths to which significant groundwater flow occurs.

Transient geotherms

Whereas one of the first papers (Suzuki 1960) on use of geotherm data, employed transient temperature conditions to calculate percolation rates in soils, by deriving an analytical solution to Eq. (7), with water-incompressibility (i.e., $\nabla \cdot \mathbf{q}=0$); such time-variant temperature profiles are less frequently investigated than their steady-state counterparts. Furthermore, the relatively rare investigations of the temporal variations in geotherms are mainly conducted on relatively shallow profiles (e.g., Suzuki 1960; Stallman

 DOI 10.1007/s10040-010-0657-2

1965; Taniguchi 1993, 1994). Many geotherms considered to be at steady-state may in fact undergo temporal changes that are not recognized because time-series measurements are rare. With the advent of distributed temperature systems (see section Geotherm measurements) transient geotherms, $T(z, t)$, may be more commonly detected.

The existence of transient processes can sometimes be inferred from analysis of a single geotherm profile at one moment in time. Such analyses are particularly useful when wells are deep and/or remotely located so that few geotherm measurements exist. Furthermore, many transient heat-transfer processes may occur over long time scales such that time-series measurements are not feasible. For example, transient conditions likely exist when a geotherm exhibits locally elevated temperatures caused by local hot lateral groundwater flow. In this conceptual model, the 1D lateral flow zone (case 2 discussed in section Steady-state geotherms) advects heat due to hot fluids sourced from depth elsewhere (Fig. 2). Confined lateral flow models were introduced by Bodvarsson et al. (1982) and built upon by Ziagos and Blackwell (1986).

For instance, to explain measured geotherm data at Long Valley Caldera, California, Blackwell (1985) applied the confined lateral flow model and attempted to remove the transient effects of hydrothermal fluid flow in the shallow (20–120 and ~700 m depth) aquifers. This analysis enables estimation of the large-scale hydrothermal flow system down to ~3 km depth, of the temporal evolution of the magmatic heat supply, and of related background heat flux rates (as further discussed in the following).

To explain measured geotherm data from Zablocki et al. (1974) at the ~1,200 m deep NSF Keller well at Kilauea Volcano in Hawaii, Hurwitz et al. (2002) explored the 2D confined lateral flow model as well as an alternative model that invoked conductive cooling of a region previously heated by advection. Previous models for Keller well temperatures had invoked a steady-state free-convection cell (Keller et al. 1979). Ultimately, Hurwitz et al. (2002) prefer the model of episodic heating with subsequent conductive cooling, which is supported by geochemical data indicating groundwater recharge at the margin of the caldera and input of magmatic gases at Halemaumau Crater (Hurwitz et al. 2003a). Both models by Hurwitz et al. (2002) are transient. The first suggests flow-zone heating toward steady-state conditions that have yet to be reached, and the second (preferred) model invokes a hot fluid injection event followed by conductive cooling. Hurwitz et al. (2002) also point out that this latter model demonstrates that even conductive regimes can be transient.

Another example of a transient geotherm is shown in Fig. 11. This profile was collected in well 35-28 in Long Valley Caldera, California, over a 17-month period in 2008–2009, employing permanently installed RTDs (see section Geotherm measurements). As in the previous example, the general shape of the profile in well 35-28 suggests advective heat transfer due to confined lateral flow at depths of approximately 119 m ($122.3<T<125.2$°C) and

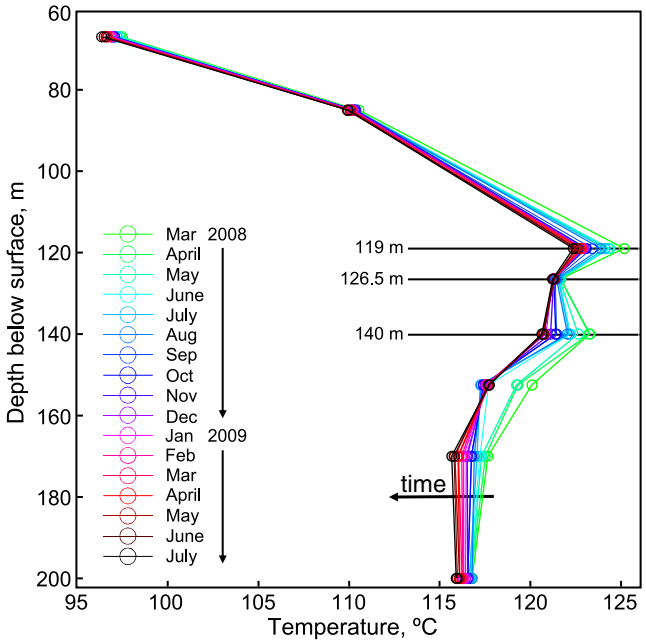

Fig. 11 Geotherms collected in borehole 35-28 within Long Valley Caldera, California, using a string of eight resistivity temperature devices (RTDs) permanently installed within the borehole (see Acknowledgements). The region of the temperature-depth profiles with highest temperatures encompasses the local hydrothermal aquifer system. Note a general cooling trend over the duration of the measurements.

140 m ($120.6<T<123.3$°C) with conductive heating above the ~119 m depth. Below ~140 m depth, as in the NSF Keller well example, conductive cooling after an episodic heating event at 140 m depth appears possible, as the time-series data indicate a continuous cooling trend. Finally, a dip in temperature at a depth of 126.5 m between the two advective heat transport zones (at 119 and 140 m depth) could be caused by advective heat transfer in a separate (i.e., at least somewhat confined), third horizontal conduit or fracture at 126.5 m depth that carries fluid at a slightly lower, and nearly constant, temperature of $121.2<T<121.7$°C. The overall cooling may be human-induced via thermal water production at a nearby geothermal power plant or it may be of a natural origin. Further research is required to accurately explain the transient temperatures at this site.

Transient processes have been recognized and modeled at Long Valley Caldera (LVC) before. The 3D model by Sorey et al. (1978) contains some analyses of transient processes. These transient models investigate the conditions under which a magma chamber could provide the heat observed today. They include a constant 800°C boundary condition at 6 km depth under the western half of the domain while, elsewhere, basal temperature was held at 300°C. Except for a discharge region at Hot Creek, surface temperature was held at 10°C, and the caldera walls imposed no-heat-flow conditions. The transient modeling results suggest that 1.5–2.5 km deep water circulation has persisted for approximately 35 ka in the western three-fifths of the caldera. More areally restricted flow regimes require deeper circulation. However, hydrothermal mineral alteration, dated at 0.3 Ma, requires hydrothermal activity at that time. The transient models

DOI 10.1007/s10040-010-0657-2

indicate lower-temperature, steady-state conditions after only about 350 ka. To maintain the observed temperatures of >200°C over such time scales would require fluid circulation depths of 4–5 km. Alternatively, Sorey et al. (1978) suggest intermittent hydrothermal activity, at 0.3 Ma and again since 35 ka, with hydrothermal activity restricted by self-sealing processes between the two events.

McKenna and Blackwell (2004) investigated the thermal behavior in Dixie Valley, Nevada, which is located in the extensional Basin and Range region, and find that it is highly time-dependent, and that the geologic history can dramatically modify the maximum geothermal reservoir temperature and its timing. They report that maximum fault-zone temperatures of 245–275°C occur early in the life of a system (at 50–60 ka) and conclude that the relatively high reservoir temperatures of over 280°C observed in some extensional geothermal systems require oscillating high/low fault permeabilities. Seismic events along these faults may be required to prevent prolonged self-sealing of faults due to mineral precipitation. Therefore, they further conclude that the maximum fault temperature may reflect the seismic recurrence interval. Their model suggests a bulk rock (i.e., non-fault) permeability of 5×10^{-16} m^2.

On shorter (i.e., decadal) time scales than those investigated by McKenna and Blackwell (2004), it appears that transient behavior of advective heat discharge at springs is less common (Ingebritsen et al. 2001). One possible explanation is that springs tend to integrate fluid-flow and heat-transfer conditions over large subsurface regions, so that the thermal conditions or the permeability field of a large region (or deep fracture) may need to change in a fundamental way to result in heat discharge variations at springs. Heat discharge at springs can provide valuable information about the subsurface thermal regime and related groundwater flow conditions, as discussed next.

Using heat discharge at springs to constrain permeabilities and groundwater flow patterns and rates

In addition to analysis of geotherms, deep and large-scale regional groundwater flow patterns may be further constrained by heat-discharge data from springs, including both hot springs like those on the western flanks of the Oregon Cascades (Fig. 7) and springs that are quite cold but nonetheless discharge significant amounts of heat.

The total heat-energy discharge per unit time is

$$Q_h = \rho_w c_w Q \Delta T, \tag{19}$$

where Q is the volumetric water flux and $\Delta T = |T_r - T_d|$ is the difference between groundwater recharge temperature, T_r, and discharge temperature, T_d. If the water discharge, Q, is large, then even small ΔT results in large heat energy discharge rates (Manga 1998). However, when constraining the magnitude of geothermal heating, it is critical to take into consideration conduction of heat to or from the Earth's surface and conversion of gravitational potential energy to heat through viscous dissipation as the groundwater moves toward lower discharge elevations (Manga and Kirchner 2004; Brumm et al. 2009). Any such heat loss or input requires addition to or subtraction from ΔT. And while discharge temperatures can easily be measured at springs, the method also requires groundwater recharge temperature to be determined—which may be challenging. Recharge temperatures are typically close to the mean annual surface temperature. Therefore, recharge temperatures may be approximated by employing stable-isotope analyses of oxygen and deuterium in spring waters. As δ^{18}O and δD decrease with elevation nearly worldwide (Poage and Chamberlain 2001), their values can often be related to recharge elevation, and thus recharge temperatures, by invoking an adiabatic lapse rate (e.g., James et al. 2000; Brumm et al. 2009).

Measurement of spring discharge, Q in Eq. (19), ranges from simple to difficult, and a variety of techniques have been proposed. One particularly useful method is the use of chloride (and sometimes sodium) to measure spring discharge into a stream (Ellis and Wilson 1955; Ingebritsen et al. 2001). Ingebritsen et al. (2001) point out that while many western United States springs do show strong seasonality, decadal trends are absent. Therefore, Ingebritsen et al. (2001) conclude that measurements of spring discharge provide a robust method for estimating advective heat transfer in the investigated regions. They find values ranging from 130 MW for the north-central Oregon Cascades to ~6,100 MW for the Yellowstone region.

The principle concept behind use of spring temperature and heat-discharge data as constraints on groundwater flow patterns is that temperatures of discharged spring water can be related to the subsurface temperatures the water encountered. Geothermal gradients, when known, can then be used to estimate the minimum depth at which such temperatures could have been encountered. If the thermal regime is poorly constrained, heat-energy measurement, Q_h, at springs, corrected for viscous heating and heat transfer from/to the Earth's surface, can help to constrain the background heat-flow rate, and, thus (if reasonable thermal conductivities are known or can be assumed), the geothermal gradient. The latter approach can be useful where background heat flow rates are masked by cold groundwater recharge. However, this approach requires some independent knowledge of groundwater-flow patterns. For example, heating by the background geothermal heat flux is only expected if a spring discharges water from the deepest flow path, as shallower flow paths may be shielded from the geothermal heat flux by deeper paths (e.g., James et al. 2000; Manga 2001; Saar et al. 2005; Fig. 8).

Furthermore, mixing of fluids that enter an upflow zone at different depths, or thermal equilibration between heated groundwater and surrounding rock, can occur while the groundwater rises through shallower, colder rock on its way to the surface (Ferguson et al. 2009). Consideration of thermal equilibration led Forster and Smith (1989) to propose that there is a country-rock permeability "window"

 DOI 10.1007/s10040-010-0657-2

of $10^{-17} \leq k \leq 10^{-15}$ m^2 that allows fault-zone hot springs to exist. If $k < 10^{-17}$ m^2, then thermal equilibration during slow water ascent will likely prevent significant advective heat discharge. If $k > 10^{-15}$ m^2, then hot springs will not occur, although significant heat can be discharged advectively, particularly when $k >> 10^{-15}$ m^2, resulting in large Q_h, despite low discharge temperatures (Manga 1998). In this case, large Q is effectively "diluting" the thermal signal, with detrimental consequences for geothermal energy resources.

In addition to heat, other natural groundwater-flow tracers such as isotopes, dissolved ions, and noble gases can help identify patterns, depths, and rates of large-scale groundwater flow (e.g., Andrews et al. 1982; James et al. 2000; Clauser et al. 2002; Evans et al. 2004; Saar et al. 2005; Kennedy and van Soest 2007; Hilton 2007). An excellent example of combining heat and other natural groundwater flow tracers to test hydrogeologic models is provided by Andrews et al. (1982), who used heat, oxygen and hydrogen isotopes, carbon isotopes, dissolved ions, and noble gas data to explore the geothermal system at Bath, England (UK). In effect employing Eq. (19) with $\rho_w = 10^3$ kg/m^3, $c_w = 4{,}180$ J/kg/°C, $Q = 10^2$ m^3/s, and $\Delta T = (70 - 25 = 45)^\circ C$, they suggest a thermal yield of $Q_h \approx 5$ MW. Based on maximum water temperatures at depth of 64–96°C (the values depend on which silica polymorph is used for the SiO_2 geothermometer) and assuming a geothermal gradient of 20°C/km, Andrews et al. (1982) estimate a groundwater circulation depth of 2,700–4,300 m at Bath. Their method depends on accurate determinations of geothermal gradients which can often be more difficult to constrain.

Like Andrews et al. (1982), James et al. (2000) use isotopes (oxygen, hydrogen, carbon, and noble gases) and heat as tracers of groundwater flow, applying the methods to small- and large-volume springs (Meinzer 1927) in the Oregon Cascades east of the crest (Fig. 7). They propose that the region is characterized by a multi-scale groundwater-flow system wherein some springs discharge groundwater from distant recharge locations, representing large-scale regional circulation, while other springs discharge local groundwater that circulated to shallow depths (Fig. 8).

Following the studies by James et al. (2000) for the Cascades and Clauser et al. (2002) for the Rhine Graben in Germany, Saar et al. (2005) investigated noble gas and heat discharge at springs on the flanks of the Cascades more closely. They find, in analogy to the conclusions by Manga (1998) and Manga and Kirchner (2004) regarding heat discharge, that magmatic helium discharge can be equally significant in the colder eastern springs, relative to the hot springs on the western flanks of the Cascades, once proper atmospheric helium corrections have been performed. The results suggest that the magmatic heat and helium source beneath the Oregon Cascades is approximately symmetric about the crest, and that asymmetric groundwater flow patterns and rates may need to be invoked to explain the significant differences in spring temperature and noble gas discharge west and east of the Cascades crest (Fig. 8).

Recently, Brumm et al. (2009) studied the heat discharge in springs in the Sierra Nevada, California, to constrain groundwater flow patterns and the background heat flux. Employing Eq. (19), and taking into account heating through viscous dissipation, they find that spring temperatures only 1–2°C above the expected mean annual temperature at the spring elevation indicate significant advective heat transfer in the Sagehen Basin and that the "basal heat flow in the Sierra Nevada may be higher than previously thought." However, they recognize an alternative scenario in which geotherm gradients are not elevated, and there is a transition from conduction to advection at shallow depths. Furthermore, they constrain groundwater circulation depths to be at least 100 m, based on time-series of spring-discharge and temperature data and an assumed conductive geotherm gradient of 10°C/km.

As alluded to in the previous, constraining background geothermal gradients, and thus water circulation depths, can be more difficult in tectonically and/or volcanologically more active regions where background heat flow rates (1) typically exceed global average rates for continental crust and (2) are often poorly constrained due to cold groundwater recharge in high-relief terrain that effectively masks the background heat flux (e.g., Forster and Smith 1989; Ingebritsen et al. 1992; Gosnold 1999). Indeed, Smith and Chapman (1983) argue that the "thermal regime within a basin with spatially varying permeability and with a structurally controlled system of aquifers will be complex." and continue that "Caution should be exercised when interpreting heat flow results in such regions as regional heat flow values." They further propose that it is more useful, in terms of background heat-flow estimations, to analyze several shallow drill holes along the hydraulic head gradient than to drill one deep borehole, unless the deep borehole reaches the conductive thermal regime below the deepest aquifer. The masking of background heat flow rates in the Oregon Cascades by cold groundwater recharge (e.g., Ingebritsen et al. 1989, 1992, 1993, 1994), for example, resulted in a controversy regarding the magnitude of lateral advective heat transfer and inferred background heat flow rates (see section Steady-state geotherms), with implications for the inferred geothermal energy potential of the region (Blackwell et al. 1982, 1990; Ingebritsen et al. 1992, 1993, 1996; Blackwell and Priest 1996).

Heat discharge at springs is a valuable metric to constrain groundwater circulation depths and large-scale flow patterns, despite the difficulties in estimating background heat flow rates and associated geothermal gradients, issues with preservation of the heat signal despite water mixing and (partial) thermal equilibration during water ascent, and complications in determining which springs sample the lowermost flow paths. The method is attractive because spring temperatures and discharge rates can be easily measured, groundwater recharge temperatures can be relatively easily inferred from $\delta^{18}O$ and δD measurements in the same spring water, and springs integrate processes over relatively large subsurface regions. The latter aspect is of particular interest here, as the theme of this paper is the use of geothermal heat as a tracer of large-scale groundwater flow and as a means to determine permeability fields over such scales. Nonetheless, and despite the associated drilling costs,

 DOI 10.1007/s10040-010-0657-2

geotherm measurements are often critical, as they can help resolve some of the problems mentioned previously. Geotherms also allow for more localized but highly sensitive measurements of groundwater flow rates and/or serve as valuable constraints in large-scale models of coupled heat and groundwater transfer. Ideally, heat transfer at springs, geotherms from boreholes, and standard hydrogeologic data are combined to allow more precise inferences of groundwater-flow velocity and permeability fields over large spatial and temporal scales.

Concluding remarks and implications

Geothermal heat has been used as a groundwater flow tracer at least since the early 1960s, and subsurface temperature fields and heat discharge at springs are highly sensitive to groundwater flow patterns and rates. Furthermore, because temperature is relatively easy, fast, and economical to measure, and because thermal material properties such as thermal conductivity and specific heat vary much less than hydraulic properties such as permeability, temperature measurements can allow much better-constrained groundwater flow or permeability estimates than hydraulic parameters alone. However, several studies reported in this review state that minimum permeabilities of approximately $5\times10^{-17}<k_{min}<10^{-15}$ m^2 are typically required to observe advective heat transfer and resultant geotherm perturbations (from linear). As discussed in this review, exact values of k_{min} depend on several other parameters such as the aspect ratio of the flow domain (basin depth to width), whether any high- or low-permeability faults or other heterogeneities are present, anisotropy of hydraulic and thermal parameters, background heat flow rates, and the shape of the water table. However, the range of possible k_{min} values is fairly narrow and located toward the lower third of geologic materials which typically exhibit permeabilities of $10^{-21}<k<10^{-7}$ m^2. Therefore, a significant fraction of naturally occurring permeabilities and groundwater flow fields can be investigated by analyzing subsurface temperature fields.

Aside from hydrogeologic insights, subsurface conductive and advective heat transfer (and related temperature distributions) also provide information on energy, climate, and other geologic systems and processes. These include magmatic intrusions and volcanic plumbing systems (e.g., Hildreth 2007), metamorphism (e.g., Manning and Ingebritsen 1999; Ingebritsen and Manning 2009), ore deposits (e.g., Garven and Freeze 1984b), global climate variability (e.g., Lachenbruch and Marshall 1986; Pollack and Huang 2000; Beltrami et al. 2005; Ferguson et al. 2006), and geothermal energy (e.g., Coolbaugh et al. 2005; Tester 2007; Kennedy and van Soest 2007; Giardini 2009; Randolph and Saar 2010).

New geotherm measurement technologies such as distributed temperature systems (see section Geotherm measurements) and constantly improving computation speeds and methods to simulate coupled groundwater and heat transfer processes over large spatial and temporal scales (e.g., Walsh et al. 2009; Ingebritsen et al. 2010; Walsh and Saar 2010; Myre et al. 2010), should result in the continued growth of the methods reviewed here, using geothermal heat as a natural groundwater flow tracer and as a means to determine permeability fields.

Acknowledgements The author thanks the generous support of the Hydrogeology and Geofluids Research Group by the George and Orpha Gibson endowment. Support for this contribution and related research is acknowledged from the National Science Foundation (NSF) under Grant Numbers EAR-0838541, DMS-0724560, and EAR-0941666 and from the Department of Energy (DOE) under Grant Number DE-EE0002764. Any opinions, findings, and conclusions or recommendations expressed in this material are those of the author and do not necessarily reflect the views of the NSF or the DOE. The data for Fig.11 were collected and processed by C. Farrar (USGS), S. Hurwitz (USGS), and J. Randolph (University of Minnesota) whose help and collaboration in coupled groundwater and geothermal heat transfer research is greatly appreciated. S. Walsh and J. Randolph are also thanked for their internal reviews of an early version of this manuscript. S. Ingebritsen and M. Person are thanked for their excellent, in-depth, and thoughtful reviews that greatly improved this paper and Editor W. Sanford for handling the review and revision process for this paper in an efficient yet patient manner.

References

Anderson MP (2005) Heat as a ground water tracer. Ground Water 43(6):951–968

Andrews JN, Burgess WG, Edmunds WM, Kay RLF, Lee DJ (1982) The thermal springs of Bath. Nature 298:339–343

Bear J (1979) Hydraulics of groundwater. McGraw-Hill, New York

Beltrami H, Ferguson G, Harris RN (2005) Long-term tracking of climate change by underground temperatures. Geophys Res Lett 32:L19707. doi:10.1029/2005GL023,714

Bense V, Beltrami H (2007) Impact of horizontal groundwater flow and localized deforestation on the development of shallow temperature anomalies. J Geophys Res 112:F04015. doi:10.1029/2006JF000,703

Bense V, Person M (2006) Faults as conduit-barrier systems to fluid flow in siliciclastic sedimentary aquifers. Water Resour Res 42: W05421. doi:10.1029/2005WR004,480

Bense V, Person M, Chaudhary K, You Y, Cremer N, Simon S (2008) Thermal anomalies indicate preferential flow along faults in unconsolidated sedimentary aquifers. Geophys Res Lett 35: L24406. doi:10.1029/2008GL036,017

Bense V, Ferguson G, Kooi H (2009) Evolution of shallow groundwater flow systems in areas of degrading permafrost. Geophys Res Lett 36:L22401. doi:10.1029/2009GL039,225

Birch F (1950) Flow of heat in the Front Range, Colorado. Bull Geol Soc Am 61:567–630

Blackwell DD (1985) A transient model of the geothermal system of Long Valley Caldera, California. J Geophys Res 90 (B13):11229–11241

Blackwell DD (1992) Geothermal and geophysical data from the Santiam Pass 77-24 well. In: Hill BE (ed) Geology and geothermal resources of the Santiam Pass Area of the Oregon Cascade Range, Deschutes, Jefferson and Linn Counties, Oregon. Open-File Report 0-92-3, Oregon Department of Geology and Mineral Industries, Salem, OR, pp 37–52

Blackwell DD, Baker SL (1988) Thermal analysis of the Austin and Breitenbush geothermal systems, Western Cascades, Oregon. In: Sherrod DR (ed) Geology and geothermal resources of the Breitenbush-Austin Hot Springs area, Clackamas and Marion counties, Oregon. Open-File Report 0-88-5, Oregon Department of Geology and Mineral Industries, Salem, OR, pp 47–62

Blackwell DD, Priest GR (1996) Comment on "Rates and patterns of groundwater flow in the Cascades Range volcanic arc and the effect on subsurface temperatures" by S. E. Ingebritsen, D. R. Sherrod, and R. H. Mainer. J Geophys Res 101(B8):17561–17568

Blackwell DD, Richards M (2004) Geothermal map of North America. 1 sheet, scale 1:6,500,000, American Association of Petroleum Geologists (AAPG), Tulsa, OK

Blackwell DD, Steele JL, Brott CA (1980) The terrain effect on terrestrial heat flow. J Geophys Res 85(B9):4757–4772

Blackwell DD, Bowen RG, Hull DA, Riccio J, Steele JL (1982) Heat-flow, arc volcanism, and subduction in northern Oregon. J Geophys Res 87(10):8735–8754

Blackwell DD, Steele JL, Frohme MK, Murphey CF, Priest GR, Black GL (1990) Heat flow in the Oregon Cascade Range and its correlation with regional gravity, Curie point depths, and geology. J Geophys Res 95(B12):19475–19493

Blythe AE, Kleinspehn KL (1998) Tectonically versus climatically driven Cenozoic exhumation of the Eurasian Plate margin, Svalbard: fission track analyses. Tectonics 17 (4):621–639

Bodri B, Rybach L (1998) Influence of topographically driven convection on heat flow in the Swiss Alps: a model study. Tectonophysics 291:19–27

Bodvarsson GS, Benson SM, Witherspoon PA (1982) Theory of the development of geothermal systems charged by vertical faults. J Geophys Res 87(B11):9317–9328

Bravo H, Feng J, Hunt R (2002) Using groundwater temperature data to constrain parameter estimation in a groundwater flow model of a wetland system. Water Resour Res 38(8):1153 . doi:10.1029/2000WR000172

Bredehoeft JD (1967) Response of well-aquifer systems to Earth tides. J Geophys Res 72(12):3075–3087

Bredehoeft J, Papadopulos IS (1965) Rates of vertical groundwater movement estimated from the Earth's thermal profile. Water Resour Res 1(2):325–328

Brott CA, Blackwell DD, Ziagos JP (1981) Thermal and tectonic implications of heat flow in the eastern Snake River Plain, Idaho. J Geophys Res 86(B12):11709–11734

Brumm M, Wang CY, Manga M (2009) Spring temperatures in the Sagehen Basin, Sierra Nevada, CA: implications for heat flow and groundwater circulation. Geofluids 9(3):195–207. doi:10.1111/j.1468–8123.2009.00,254.x

Buck WR, Martinez F, Steckler MS, Cochran JR (1988) Thermal consequences of lithospheric extension: pure and simple. Tectonophysics 7(2):213–234

Carslaw HS, Jaeger JC (1959) Conduction of heat in solids, 2nd edn. Oxford University Press, Oxford, UK

Cartwright K (1970) Groundwater discharge in the Illinois Basin as suggested by temperature anomalies. Water Resour Res 6(3):912–918

Cermaka V, Bodrib L, Safanda J (2009) Tidal modulation of temperature oscillations monitored in borehole Yaxcopoil-1 (Yucatan, Mexico). Earth Planet Sci Lett 282(1–4):131–139

Christiansen LB, Hurwitz S, Saar MO, Ingebritsen SE, Hsieh PA (2005) Seasonal seismicity at western United States volcanic centers. Earth Planet Sci Lett 240(2):307–321

Clauser C, Griesshaber E, Neugebauer HJ (2002) Decoupled thermal and mantle helium anomalies: implications for the transport regime in continental rift zones. J Geophys Res 107. doi:10.1029/2001JB000,675

Constantz J (2008) Heat as a tracer to determine streambed water exchanges. Water Resour Res 44:W00D10. doi:10.1029/2008WR006,996

Coolbaugh M, Arehart G, Faulds J, Garside L (2005) Geothermal systems in the Great Basin, western United States: modern analogues to the role of magmatism, structure, and regional tectonics in the formation of gold deposits. Geological Society of Nevada Symposium 2005: Window to the World, Reno, Nevada, May 2005, pp 1063–1081

Darcy HPG (1856) Les fountaines publiques de la Ville de Dijon [The public fountains of the city of Dijon]. Dalmont, Paris

Deming D (1993) Regional permeability estimates from investigations of coupled heat and groundwater flow, North Slope of Alaska. J Geophys Res 98:16271–16286

Deming D, Nunn J (1991) Numerical simulations of brine migration by topographically driven recharge. J Geophys Res 96 (B2):2485–2499

Domenico PA, Palciauskas VV (1973) Theoretical analysis of forced convective heat transfer in regional ground-water flow. Geol Soc Am Bull 84:3803–3814

Ellis AJ, Wilson SH (1955) The heat from the Wairakei-Taupo thermal region calculated from the chloride output. NZ J Sci Technol B36:622–631

Evans WC, van Soest MC, Mariner RH, Hurwitz S, Ingebritsen SE, Wicks CW Jr, Schmidt ME (2004) Magmatic intrusion west of Three Sisters, central Oregon, USA: the perspective from spring geochemistry. Geology 32(1):69–72

Fairley J, Hinds J (2004) Rapid transport pathways for geothermal fluids in an active Great Basin fault zone. Geology 32(9):825–828

Ferguson G, Beltrami H (2006) Transient lateral heat flow due to land-use changes. 242(1–2):217–222

Ferguson G, Woodbury AD (2007) Urban heat island in the subsurface. Geophys Res Lett 34:L23713. doi:10.1029/2007GL032,324

Ferguson G, Beltrami H, Woodbury AD (2006) Perturbation of ground surface temperature reconstruction by groundwater flow. Geophys Res Lett 33:L13708. doi:10.1020/2006GL026,634

Ferguson G, Grasby SE, Hindle SR (2009) What do aqueous geothermometers really tell us? Geofluids 9(1):39–48

Forster C, Smith L (1988a) Groundwater flow systems in mountainous terrain 1: numerical modeling technique. Water Resour Res 24(7):999–1010

Forster C, Smith L (1988b) Groundwater flow systems in mountainous terrain 2: controlling factors. Water Resour Res 24(7):1011–1023

Forster C, Smith L (1989) The influence of groundwater flow on thermal regimes in mountainous terrain: a model study. J Geophys Res 94:9439–9451

Fourier JBJ (1822) Theorie Analytique de la Chaleur [The analytical theory of heat]. Didot, Paris

Freeze RA, Cherry JA (1979) Groundwater. Prentice Hall, Englewood Cliffs, NJ

Furbish DJ (1997) Fluid physics in geology. Oxford University Press, Oxford, UK

Garven G, Freeze R (1984a) Theoretical analysis of the role of groundwater flow in the genesis of stratabound ore deposits. 1. Mathematical and numerical model. Am J Sci 284(10):1085–1124

Garven G, Freeze R (1984b) Theoretical analysis of the role of groundwater flow in the genesis of stratabound ore deposits. 2. Quantitative results. Am J Sci 284(10):1125–1174

Ge S (1998) Estimation of groundwater velocity in localized fracture zones from well temperature profiles. J Volcanol Geoth Res 84:93–101

Germanovich LN, Lowell RP, Astakhov DK (2000) Stress-dependent permeability and the formation of seafloor event plumes. JGR 105:8341–8354

Giardini D (2009) Geothermal quake risks must be faced. Nature 462:848–849

Gosnold WD (1985) Heat flow and ground water flow in the Great Plains of the United States. J Geodyn 4:247–264

Gosnold WD (1990) Heat flow in the Great Plains of the United States. J Geophys Res 95(B1):353–374

Gosnold WD (1999) Basin-scale groundwater flow and advective heat flow: an example from the Northern Great Plains. In: Basin analysis. Kluwer, Dordrecht, The Netherlands, pp 99–116

Herbert A, Jackson C, Lever D (1988) Coupled groundwater flow and solute transport with fluid density strongly dependent upon concentration. Water Resour Res 24(10):1781–1795

Hildreth W (2007) Quaternary magmatism in the Cascades; geologic perspectives. US Geol Surv Prof Pap P1744, 125 pp

Hilton D (2007) The leaking mantle. Science 318:1389–1390

Hsieh PA (1998) Scale effects in fluid flow through fractured geologic media. In: Sposito G (ed) Scale dependence and scale invariance in hydrology. Cambridge University Press, New York, pp 335–353
Hsieh PA, Bredehoeft JD, Rojstaczer SA (1988) Response of well aquifer systems to Earth tides: problem revisited. Water Resour Res 24(3):468–472
Hurwitz S, Ingebritsen SE, Sorey ML (2002) Episodic thermal perturbations associated with groundwater flow: an example from Kilauea volcano, Hawaii. J Geophys Res 107:2297
Hurwitz S, Goff F, Janik CJ, Evans WC, Counce DA, Sorey ML, Ingebritsen SE (2003a) Mixing of magmatic volatiles with groundwater and interaction with basalt on the summit of Kilauea Volcano, Hawaii. J Geophys Res 108(B1):ECV8.1–ECV8.12
Hurwitz S, Kipp KL, Ingebritsen SE, Reid ME (2003b) Groundwater flow, heat transport, and water table position within volcanic edifices: implications for volcanic processes in the Cascade range. J Geophys Res 108:ECV1.1–ECV1.19. doi:10.1029/2003JB002,565
Hyun Y, Neuman SP, Vesselinov VV, Illman WA, Tartakovsky DM, Di Federico V (2002) Theoretical interpretation of a pronounced permeability scale effect in unsaturated fractured tuff. Water Resour Res 38(6):1092
Ingebritsen SE, Manning C (2009) Permeability of the continental crust: dynamic variations inferred from seismicity and metamorphism. Geofluids 10:193–205. doi:10.1111/j.1468-8123.2010.00278.x
Ingebritsen SE, Sherrod DR, Mariner RH (1989) Heat-flow and hydrothermal circulation in the Cascade Range, north-central Oregon. Science 243(4897):1458–1462
Ingebritsen SE, Sherrod DR, Mariner RH (1992) Rates and patterns of groundwater flow in the Cascade Range Volcanic Arc, and the effect on subsurface temperatures. J Geophys Res 97:4599–4627
Ingebritsen SE, Scholl MA, Sherrod DR (1993) Heat flow from four new research drill holes in the Western Cascades, Oregon, U.S.A. Geothermics 22(3):151–163
Ingebritsen SE, Mariner RH, Sherrod DR (1994) Hydrothermal systems of the Cascades Range, north-central Oregon. US Geol Surv Prof Pap 1044-L
Ingebritsen SE, Sherrod DR, Mariner RH (1996) Reply to comment on "Rates and patterns of groundwater flow in the Cascades Range volcanic arc and the effect on subsurface temperatures". J Geophys Res 101(B8):17569–17576
Ingebritsen SE, Galloway DL, Colvard EM, Sorey ML, Mariner RH (2001) Time-variation of hydrothermal discharge at selected sites in the western United States: implications for monitoring. J Volcanol Geoth Res 111(1–4):1–23
Ingebritsen SE, Sanford W, Neuzil C (2006) Groundwater in geologic processes, 2nd edn. Cambridge University Press, Cambridge, UK
Ingebritsen SE, Geiger S, Hurwitz S, Driesner T (2010) Numerical simulation of magmatic hydrothermal systems. Rev Geophys 48:RG1002. doi:10.1029/2009RG000,287
James EW, Manga M, Rose TP, Hudson GB (2000) The use of temperature and the isotopes of O H C and noble gases to determine the pattern and spatial extent of groundwater flow. J Hydrol 237:100–112
Jessop AM (1989) Hydrological distortion of heat flow in sedimentary basins. Tectonophysics 164:211–218
Keller GV, Grose LT, Murray JC, Skokan CK (1979) Results of an experimental drill hole at the summit of Kilauea Volcano, Hawaii. J Volcanol Geoth Res 5(3–4):345–385
Kennedy B, van Soest M (2007) Flow of mantle fluids through the ductile lower crust: helium isotope trends. Science 318:1433–1436
Kestin J, Khalifa H, Correia R (1981) Tables of the dynamic and kinematic viscosity of aqueous NaCl solutions in the temperature range 20–150°C and the pressure range 0.1–35MPa. J Phys Chem Ref Data 10(1):71–87
Lachenbruch AH (1968) Rapid estimation of the topographic disturbance to superficial thermal gradients. Rev Geophys 6 (3):365–400
Lachenbruch AH, Marshall BV (1986) Changing climate: geothermal evidence from permafrost in the Alaskan Arctic. Science 234(4777):689–696
López DL, Smith L (1995) Fluid flow in fault zones: analysis of the interplay of convective circulation and topographically driven groundwater flow. Water Resour Res 31(6):1489–1503
López DL, Smith L (1996) Fluid flow in fault zones: influence of hydraulic anisotropy and heterogeneity on the fluid flow and heat transfer regime. Water Resour Res 32(10):3227–3235
Lu N, Ge S (1996) Effect of horizontal heat and fluid flow on the vertical temperature distribution in a semiconfining layer. Water Resour Res 32(5):1449–1453
Manga M (1998) Advective heat transport by low-temperature discharge in the Oregon Cascades. Geology 26(9):799–802
Manga M (2001) Using springs to study groundwater flow and active geologic processes. Annu Rev Earth Planet Sci 29:201–228
Manga M, Kirchner JW (2004) Interpreting the temperature of water at cold springs and the importance of gravitational potential energy. Water Resour Res 40(5):W05110.1–W05110.8. doi:10.1029/2004WR002,905
Manning CE, Ingebritsen SE (1999) Permeability of the continental crust: implications of geothermal data and metamorphic systems. Rev Geophys 37:127–150
McCord J, Reiter M, Phillips F (1992) Heat-flow data suggest large ground-water fluxes through Fruitland coals of the northern San Juan basin, Colorado-New Mexico. Geology 20:419–422
McKenna JR, Blackwell DD (2004) Numerical modeling of transient basin and range extensional geothermal systems. Geothermics 33(4):457–476
McKenzie J, Voss C, Siegel D (2007) Groundwater flow with energy transport and water-ice phase change: numerical simulations, benchmarks, and application to freezing in peat bogs. Adv Water Resour 30(4):966–983
Meinzer OE (1927) Large springs in the United States. US Geol Surv Water Supp Pap 557:94
Myre J, Walsh SDC, Lilja DJ, Saar MO (2010) Performance analysis of single-phase, multiphase, and multicomponent lattice-Boltzmann fluid flow simulations on GPU clusters. Concurrency Computat Pract Exper. doi:10.1002/cpe.1645
Perkins TK, Johnston OC (1963) A review of diffusion and dispersion in porous media. Soc Pet Eng J 3:70–83
Person M, Mulch A, Teyssier C, Gao Y (2007) Isotope transport and exchange within metamorphic core complexes. Am J Sci 307. doi:10.247/03.2007.01
Person M, Banerjee A, Hofstra A, Sweetkind D, Gao Y (2008) Hydrologic models of modern and fossil geothermal systems in the Great Basin: genetic implications for epithermal Au–Ag and Carlin-type gold deposits. Geosphere 4(5):888–917
Phillips OM (1991) Flow and reactions in permeable rocks. Cambridge University Press, New York
Poage MA, Chamberlain CP (2001) Empirical relationships between elevation and the stable isotope composition of precipitation and surface waters: considerations for studies of paleoelevation change. Am J Sci 301(1):1–15
Pollack HN, Huang S (2000) Climate reconstruction from subsurface temperatures. Annu Rev Earth Planet Sci 28:339–365
Pollack HN, Hurter SJ, Johnson JR (1993) Heat-flow from the Earth's interior: analysis of the global data set. Rev Geophys 31 (3):267–280
Pollack HN, Smerdon J, Keken PE (2005) Variable seasonal coupling between air and ground temperatures: a simple representation in terms of subsurface thermal diffusivity. Geophys Res Lett 32:L15405. doi:10.1029/2005GL023,869
Randolph J, Saar M (2010) Coupling geothermal energy capture with carbon dioxide sequestration in naturally permeable, porous geologic formations: a comparison with enhanced geothermal systems. GRC Transaction, Geothermal Resources Council, Davis, CA
Rath V, Wolf A, Bücker H (2006) Joint three-dimensional inversion of coupled ground-water flow and heat transfer based on automatic differentiation: sensitivity calculation, verification, and synthetic examples. Geophys J Int 167(1):453–466

Rinehart JS (1972) Fluctuations in geyser activity caused by variations in Earth tidal forces, barometric pressure, and tectonic stresses. J Geophys Res 77(2):342–350

Rye DM, Roy RF (1978) The distribution of thorium, uranium, and potassium in Archean Granites from northeastern Minnesota. Am J Sci 278:354–378

Saar MO, Manga M (1999) Permeability-porosity relationship in vesicular basalts. Geophys Res Lett 26(1):111–114

Saar MO, Manga M (2003) Seismicity induced by seasonal groundwater recharge at Mt. Hood, Oregon. Earth Planet Sci Lett 214(3–4):605–618

Saar MO, Manga M (2004) Depth dependence of permeability in the Oregon Cascades inferred from hydrogeologic, thermal, seismic, and magmatic modeling constraints. J Geophys Res 109:B04204. doi:10.1029/2003JB002855

Saar MO, Castro MC, Hall CM, Manga M, Rose TP (2005) Quantifying magmatic, crustal, and atmospheric helium contributions to volcanic aquifers using all stable noble gases: implications for magmatism and groundwater flow. Geochem Geophys Geosys 6(3):Q03008. doi:10.1029/2004GC000828

Sánchez-Vila X, Carrera J, Girardi J (1996) Scale effects in transmissivity. J Hydrol 183(1–2):1–22

Sass JH, Lachenbruch AH, Munroe RJ (1971) Thermal conductivity of rocks from measurements on fragments and its application to heat-flow determinations. J Geophys Res 76:3391–3401

Smerdon JE, Pollack HN, Enz JW, Lewis MJ (2003) Conduction-dominated heat transport of the annual temperature signal in soil. J Geophys Res 108(B9). doi:10.1029/2002JB002,351

Smith L, Chapman DS (1983) On the thermal effects of groundwater flow 1: regional scale systems. J Geophys Res 88:593–608

Smith L, Chapman D (1985) The influence of water table configuration on the near-surface thermal regime. J Geodyn 4:183–198

Sorey ML (1971) Measurement of vertical groundwater velocity from temperature profiles in wells. Water Resour Res 7(4):963–970

Sorey ML (1976) A model of the hydrothermal system of Long Valley Caldera, California. Paper presented at the Second Workshop on Geothermal Reservoir Engineering. Stanford University, Stanford, CA, December 1976

Sorey ML, Lewis RE, Olmsted FH (1978) The hydrothermal system of Long Valley Calderra, California. US Geol Surv Prof Pap 1044-A

Stallman RW (1963) Computation of ground-water velocity from temperature data. In: Bentall R (ed) Methods of collecting and interpreting ground-water data. US Geol Surv Water Suppl Pap 1544-H. pp 36–46

Stallman RW (1965) Steady one-dimensional fluid flow in a semi-infinite porous medium with sinusoidal surface temperature. J Geophys Res 70(12):2821–2827

Steele JL, Blackwell DD (1982) Heat flow in the vicinity of the Mount Hood volcano, Oregon. In: Priest GR, Vogt BF (eds) Geology and geothermal resources of the Mount Hood area, Oregon. Special paper 14. Oregon Department of Geology and Mineral Industries, Portland, OR, pp 31–42

Stonestrom DA, Constantz J (2003) Heat as a tool for studying the movement of ground water near streams. US Geol Surv Circ 1260, 96 pp

Suzuki S (1960) Percolation measurements based on heat flow through soil with special reference to paddy fields. J Geophys Res 65(9):2883–2885

Taniguchi M (1993) Evaluation of vertical groundwater fluxes and thermal properties of aquifers based on transient temperature-depth profiles. Water Resour Res 29(7):2021–2026

Taniguchi M (1994) Estimated recharge rates from groundwater temperatures in the Nara Basin, Japan. Hydrogeol J 2(4)7–14. doi:10.1007/s100400050,031

Taniguchi M, Shimada J, Tanaka T, Kayane I, Sakura Y, Shimano Y, Dapaah-Siakwan S, Kawashima S (1999a) Disturbances of temperature-depth profiles due to surface climate change and subsurface water flow: 1, an effect of linear increase in surface temperature caused by global warming and urbanization in the Tokyo metropolitan area, Japan. Water Resour Res 35(5):1507–1517

Taniguchi M, Williamson DR, Peck AJ (1999b) Disturbances of temperature-depth profiles due to surface climate change and subsurface water flow: 2, an effect of step increase in surface temperature caused by forest clearing in southwest-western Australia. Water Resour Res 35(5):1519–1529

Tester J (2007) The future of geothermal energy: impact of enhanced geothermal systems (EGS) on the United States in the 21st Century. Technical report, Massachusetts Institute of Technology, Boston

Turcotte DL, Schubert G (2002) Geodynamics. Cambridge University Press, Cambridge, UK

Tyler S, Selker J, Hausner M, Hatch C, Torgersen T, Thodal C, Schladow S (2009) Environmental temperature sensing using Raman spectra DTS fiber-optic methods. Water Resour Res 45: W00D23. doi:10.1029/2008WR007,052

Walsh SDC, Saar MO (2010) Macroscale lattice-Boltzmann methods for low Peclet number solute and heat transport in heterogeneous porous media. Water Resour Res 46:W07517. doi:10.1029/2009WR007895

Walsh SDC, Saar MO, Bailey P, Lilja DJ (2009) Accelerating geoscience and engineering system simulations on graphics hardware. Comput Geosci 35(12):2353–2364

Walvoord M, Striegl R (2007) Increased groundwater to stream discharge from permafrost thawing in the Yukon River basin: potential impacts on lateral export of carbon and nitrogen. Geophys Res Lett 34:L12402. doi:10.1029/2007GL030,216

Wisian KW, Blackwell DD, Bellani S, Henfling JA, Normann RA, Lysne PC, Foerster A, Schroetter J (1998) Field comparison of conventional and new technology temperature logging systems. Geothermics 27(2):131–141

Woodbury AD, Smith L (1985) On the thermal effects of three-dimensional groundwater flow. J Geophys Res 90(B1):759–767

Woodbury AD, Smith L (1988) Simultaneous inversion of hydrogeologic and thermal data: 2. incorporation of thermal data. Water Resour Res 24(3):356–372

Woodbury AD, Smith L, Dunbar WS (1987) Simultaneous inversion of hydrogeologic and thermal data: 1. theory and application using hydraulic head data. Water Resour Res 23 (8):1586–1606

Zablocki CJ, Tilling RI, Peterson DW, Christiansen RL, Keller GV, Murray JC (1974) A deep research drill hole at the summit of an active volcano, Kilauea, Hawaii. Geophys Res Lett 1(7):323–326

Zeitler PK, Koons PO, Bishop MP, Chamberlain CP, Craw D, Edwards MA, Hamidullah S, Jan MQ, Khan MA, Khattak MUK, Kidd WSF, Mackie RL, Meltzer AS, Park SK, Pecher A, Poage MA, Sarker G, Schneider DA, Seeber L, Shroder JF (2001) Crustal reworking at Nanga Parbat, Pakistan: metamorphic consequences of thermal-mechanical coupling facilitated by erosion. Tectonics 20(5):712–728

Ziagos JP, Blackwell DD (1986) A model for the transient temperature effects of horizontal fluid flow in geothermal systems. J Volcanol Geoth Res 27:371–397